Hindawi
Shock and Vibration
Volume 2020, Article ID 1417969, 21 pages
https://doi.org/10.1155/2020/1417969

Research Article

Earthquake Response Analysis of Tall Reinforced Concrete Chimneys considering Eccentricity

Yingchun Jiang,[1] **Tielin Liu**,[2] **and Yikui Bai**[3]

[1]*College of Engineering, Shenyang Agricultural University, Shenyang 110866, China*
[2]*School of Civil Engineering, Shenyang Jianzhu University, Shenyang 110168, China*
[3]*College of Water Conservancy, Shenyang Agricultural University, Shenyang 110866, China*

Correspondence should be addressed to Yingchun Jiang; jyclg@syau.edu.cn

Received 14 October 2019; Revised 7 January 2020; Accepted 29 January 2020; Published 11 March 2020

Academic Editor: Salvatore Caddemi

A numerical algorithm is presented to analyze earthquake response of tall reinforced concrete (RC) chimneys based on stick multidegree-of-freedom models. The algorithm considers the eccentricity phenomena between spatial discrete nodes and corresponding centroids of investigated lumps. The spatial discrete segments of the chimney are used to construct the investigated lumps. The equations of dynamic equilibrium of the investigated lumps are derived, and the numerical calculation procedure is implemented. Phenomena of eccentricity are studied for 150 m and 210 m RC chimneys. Seismic stresses and effects of vertical ground motion for the two chimneys are also studied. Numerical results show that the tensile and compressive stresses of the seismic control cross sections of the chimneys may increase under the actions of several specific earthquake waves by considering existing eccentricities. The effect of eccentricity on the earthquake responses of tall RC chimney should be considered, and stresses caused by vertical ground motion should not be neglected to obtain accurate earthquake response of chimneys.

1. Introduction

1.1. Literature Review. Many tall reinforced concrete (RC) chimneys have been built in places such as coal-fired power stations and refinery because of the requirements of air pollution control standards. Slender tall chimneys are sensitive to earthquake. Strong earthquake threatens the safety of the chimney and other buildings around it because of the nonuniformity of the diameter along the height of the chimney and the variation in dead weights at different heights. Research and calculations of earthquake response are necessary for the designs of tall RC chimneys under the action of earthquakes.

Destruction and collapse of tall chimneys bring huge economic losses. Research on seismic damage of chimneys indicates that the destructive effect of vertical earthquake on chimneys should be considered [1]. Liu and He [2] analyzed the seismic response of a chimney under the action of combined horizontal and vertical ground motions. They concluded that vertical stress cannot be neglected completely although horizontal seismic stress is the controlling part. Wang and Liao [3] developed a calculation technique for analyzing the vertical earthquake response of a chimney based on multiple reflections of traveling waves in the chimney. Liu et al. [4] conducted earthquake transient response of multidegree-of-freedom (MDOF) systems by the model superposition method. Ding et al. [5] conducted a vertical impact to the bottoms of chimney models. The test results showed that only one circle crack appeared in the chimney models, and the crack had relations with the ratio of input wave frequency to the natural frequency of the chimney model. Chen et al. [6] used a shaking table to study the fracture phenomenon of a chimney under the action of vertical earthquake. They found that vertical seismic action should be considered in the structural design of chimneys.

A 115 m high RC chimney collapsed on August 17, 1999, during the Izmit earthquake in Turkey [7–10]. Huang et al. [7, 8] investigated a collapsed chimney with methods of

linear dynamic response spectrum and nonlinear static capacity spectrum. Akinci [9] used shell elements to analyze a collapsed chimney. The analysis results indicated that low ductility and inadequate capacity due to a large duct were the two significant factors for the collapsed chimney. Huang and Gould [10] further proposed a new three-dimensional (3-D) pushover analysis method to study the dynamic response of the stack due to an earthquake motion recorded at a nearby site. Lopes et al. [11] constructed a realistic numerical model to evaluate the seismic vulnerability of a chimney and simulated its damaged state. Minghini et al. [12] analyzed a brickwork chimney and a shear failure mechanism of the upper part of the chimney damaged by the 2012 Emilia earthquake. Zhou et al. selected an existing 240 m tall RC chimney as the research object and analyzed the seismic vulnerability curve of the chimney by considering structural damage [13], structural nonlinearity [14], and multidimensional earthquake [15] and evaluated and analyzed the vulnerability of the chimney structure.

The modal frequency and mode shape are the main dynamic characteristics of chimneys. Chen et al. [16] used the Adomian decomposition method to decompose dimensionless modal shape and calculated the dynamic characteristics of a high-rise chimney. Sancibrian et al. [17] used the continuum structure system to analyze the dynamic characteristics of a chimney, including natural frequencies and mode shapes. Tatara and Ratajewicz [18] evaluated the dynamic characteristics of a typical RC industrial chimney that belongs to a heating plant and determined the lowest vibration frequency of the structure.

Soil-structure interaction (SSI) has a great influence on the seismic performance of tall chimney structures [19, 20]. Halabian and Kabiri [21] studied the effect of foundation stiffness of different types of RC chimneys on the ductility reduction coefficient. A series of inelastic and elastic time history analyses up to the collapse status for a large variety of RC chimneys subjected to five scaled artificial records were conducted. Jisha et al. [22] analyzed 3-D SSI of tall RC chimneys with annular raft foundation and evaluated the effect of SSI by changing the stiffness of supporting soil and foundation [23]. Zhou et al. [24, 25] studied the effect of SSI on the seismic collapse resistance of chimney structure for a 240 m high RC chimney.

Time period is an important approach of evaluating the structural response of a structure subjected to large-scale earthquake vibrations. The seismic response of chimney structures uses time history analysis considering earthquake, which is a long-duration earthquake impulse [19]. Sarkar et al. [26] studied the effects of different base conditions on the design value of shear force and bending moment of different sections of a 275 m tall RCC multiflue chimney by using a response spectrum method. The spectrum compatibility time history of specific engineering site was considered, and the time history dynamic analysis of the chimney structure was conducted in detail. Wilson [27] studied the inelastic response of 10 RC chimneys ranging from 115 m to 301 m subject to earthquake excitation. Liu et al. [28] studied the structural dynamic performance and elastic-plastic seismic response of a 240 m high special-shaped RC chimney. The weak position of the chimney was discussed by analyzing its interlayer displacement angle.

1.2. Motivation. When the stick MDOF structural model is used to study the dynamic response of tall chimney structures, the chimney structure is usually discretized into beam elements of a certain length. Thin beam elements are good, but they are not sufficiently thin in practical analysis. The cross section area of a chimney structure is variable at different heights. Therefore, even if the discrete length of space is equal, the vertical eccentricity of mass will occur because the mass of each element will be uneven. The vertical eccentricity of mass must be considered to improve the accuracy and validity of dynamic response analysis.

A numerical algorithm is presented in this study to analyze the earthquake response of tall RC chimneys. The chimney is spatially discretized into several segments of finite length, and the investigated lumps are then constructed by using these segments. The calculating formulae of axial force, shear force, and bending moment acting on the median cross section of each segment are derived. These interior forces are associated with end displacement and angle. Not only the inertial forces of the investigated lumps are considered but also the rotary inertias of investigated lumps. Existing eccentricity phenomena between spatial discrete nodes and corresponding centroids of investigated lumps are considered. Dynamic equations and relations are applied alternately in the time domain to calculate the seismic response of the chimney. Two RC chimneys of 150 m and 210 m height are studied. The numerical results show that the effects of such eccentricities on earthquake response should not be neglected for tall chimneys, as well as the vertical ground motion.

2. Numerical Algorithm

2.1. Governing Equations of Investigated Lumps. A chimney with variable cross section can be discretized into many segments of different cross section areas along the vertical direction in practical calculation based on the stick MDOF model. These segments are used to construct the investigated lumps. Figure 1 shows a typical investigated lump i (the nodal numbering i is also used to describe the investigated lump) consisting of half the upper segment and half the lower segment around the discrete node i. Sign C is the centroid of the investigated lump. The centroid of the investigated lump is commonly not at the same point of the corresponding discrete node i for the chimney with variable cross-sectional area. Here, the distance between the discrete node and the centroid of the investigated lump within the same investigated lump is called eccentricity.

The vertical equilibrium equation for the centroid of investigated lump i is

$$m_i \ddot{w}_{ci} = N_{l-1} - N_l - m_i g, \tag{1}$$

where m_i is the mass of investigated lump i, $\ddot{w}_{ci}$ is the vertical acceleration of centroid C, and N_{l-1} and N_l are the axial forces acting on investigated lump i.

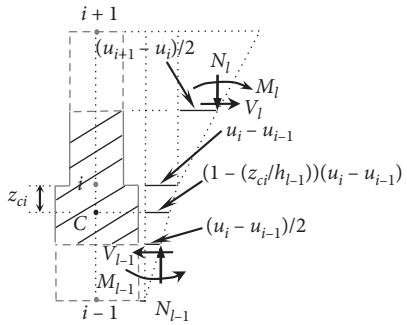

Figure 1: Sketch of deformation of investigated lump i.

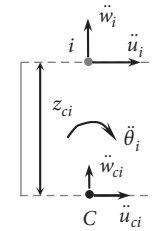

Figure 2: Accelerations of node i and centroid C of the investigated lump.

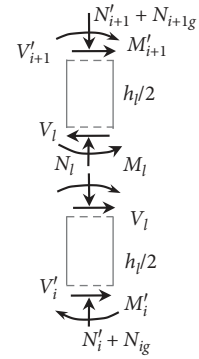

Figure 3: Free-body diagrams of segment l.

The transverse equilibrium equation for the centroid of investigated lump i is

$$m_i \ddot{u}_{ci} = V_l - V_{l-1}, \tag{2}$$

where $\ddot{u}_{ci}$ is the horizontal acceleration of the centroid of investigated lump i and V_l and V_{l-1} are the shear forces acting on investigated lump i.

On the basis of mechanics theory, the rotational equilibrium equation should be established about the horizontal axis (y-axis) through centroid C of investigated lump i, that is,

$$J_{ci}\ddot{\theta}_i = (M_l - M_{l-1}) + V_l\left(\frac{h_l}{2} + z_{ci}\right) + V_{l-1}\left(\frac{h_{l-1}}{2} - z_{ci}\right) + N_l\left[\frac{u_{i+1} - u_i}{2} + \frac{z_{ci}(u_i - u_{i-1})}{h_{l-1}}\right] + N_{l-1}\left(\frac{1}{2} - \frac{z_{ci}}{h_{l-1}}\right)(u_i - u_{i-1}), \tag{3}$$

where J_{ci} is the moment of inertia of investigated lump i about the y-axis through its centroid; $\ddot{\theta}_i$ and z_{ci} are the angular acceleration and the eccentricity of investigated lump i, respectively; M_l and h_l are the bending moments and the length of segment l, respectively; and u_i is the transverse displacement of node i.

Figure 2 shows that the following relation holds:

$$\ddot{u}_i = \ddot{u}_{ci} + z_{ci}\ddot{\theta}_i, \tag{4}$$

where $\ddot{u}_i$ is the horizontal acceleration of node i. In Figure 2, $\ddot{w}_i$ is the vertical acceleration of node i.

2.2. Forces and Bending Moment on the Central Cross Section of the Segment. Figure 3 shows the free-body diagrams of the upper and lower halves of segment l by an artificial cut at the central section of segment l. In Figure 3, N'_i and N'_{i+1} are the axial compressive forces at the bottom and top ends of segment l, respectively, because of its vertical deformation; V'_i and V'_{i+1} are the shear forces; M'_i and M'_{i+1} are the bending moments; N_{ig} is the axial force coming from the dead load of the structure above node i; and N_{i+1g} is the dead load above node $i + 1$.

Following the beam theory considering shear deformation and axial force, we have

$$N'_{i+1} = N'_i = \frac{(EA)_l}{h_l}(w_i - w_{i+1}), \tag{5}$$

$$V'_{i+1} = -V'_i = K_{1l}(u_{i+1} - u_i) + K_{2l}(\theta_i + \theta_{i+1}), \tag{6}$$

$$M'_i = K_{2l}(u_{i+1} - u_i) + K_{3l}\theta_i + K_{4l}\theta_{i+1}, \tag{7}$$

$$M'_{i+1} = K_{2l}(u_{i+1} - u_i) + K_{4l}\theta_i + K_{3l}\theta_{i+1}, \tag{8}$$

where $K_{1l} = (12(\mathrm{EI})_l/h_l^3(1 + 2\alpha_l)) - (6N_l/5h_l)$, $K_{2l} = -(6(\mathrm{EI})_l/h_l^2(1 + 2\alpha_l)) + (N_l/10)$, $K_{3l} = (4(1 + 0.5\alpha_l)(\mathrm{EI})_l/h_l(1 + 2\alpha_l)) - (2N_l h_l/15)$, and $K_{4l} = (2(1 - \alpha_l)(\mathrm{EI})_l/h_l(1 + 2\alpha_l)) + (N_l h_l/30)$. Subscript l denotes the l^{th} segment. $\alpha_l = 6(\mathrm{EI})_l/[h_l^2(\mathrm{GA})_l]$ is the coefficient of shear deformation in the transverse direction. $(\mathrm{EI})_l$, $(\mathrm{GA})_l$, and $(\mathrm{EA})_l$ are the bending stiffness, shear stiffness, and tensile/compressive stiffness of segment l, respectively. $N_l = N_{ig} + N'_i$, where N_{ig} is the axial force coming from the dead weight of the chimney above node i. A_l is the cross-sectional area of segment l. w_i and θ_i are the vertical displacement and rotational angle of node i, respectively. w_{i+1} and θ_{i+1} are the vertical displacement and rotational angle of node $i + 1$, respectively.

Subtracting equation (8) from equation (7) yields

$$M'_i - M'_{i+1} = \left[\frac{2(EI)_l}{h_l} - \frac{N_l h_l}{6}\right](\theta_i - \theta_{i+1}). \tag{9}$$

Given the equilibrium of the upper half of segment l, we have

$$M'_{i+1} = M_l - V_l\frac{h_l}{2} - N_l\frac{u_{i+1}-u_i}{2}, \tag{10}$$

$$V_l = K_{1l}(u_{i+1}-u_i) + K_{2l}(\theta_i+\theta_{i+1}). \tag{11}$$

Given the equilibrium of the lower half of segment l, we have

$$M'_i = -M_l - V_l\frac{h_l}{2} - N_l\frac{u_{i+1}-u_i}{2}, \tag{12}$$

where N_l, V_l, and M_l are the central axial force, central shear force, and central bending moment acting on the central section of segment l, respectively.

We substitute equations (10) and (12) into equation (9), and we obtain the central bending moment of segment l, shown as follows:

$$M_l = K_{5l}(\theta_{i+1}-\theta_i), \tag{13}$$

where $K_{5l} = ((\mathrm{EI})_l/h_l) - (N_l h_l/12)$.

2.3. Implementation of Algorithm. Horizontal and vertical earthquake waves are inputted from the foundation of the tall RC chimney. The algorithm description diagram is shown in Figure 4, and the calculating procedure is as follows.

Step 1. Calculate the angular acceleration $\ddot{\theta}_i$ of investigated lump i at time t using equation (3), the vertical acceleration $\ddot{w}_{ci}$ at time t using equation (1), $\ddot{w}_i$ at time t by considering $\ddot{w}_i$ being nearly equal to $\ddot{w}_{ci}$, the horizontal acceleration $\ddot{u}_{ci}$ at time t using equation (2), and $\ddot{u}_i$ using equation (4).

Step 2. Calculate angle θ_i, vertical displacement w_i, and horizontal displacement u_i for investigated lump i at time $t+\Delta t$ by integration in the time domain.

Step 3. Calculate axial force N'_i at time $t+\Delta t$ using equation (5) and then obtain central axial force N_l using the formula $N_l = N_{ig} + N'_i$. Central shear force V_l and central bending moment M_l are calculated using equations (11) and (13), respectively, at time $t+\Delta t$.

Step 4. Calculate $\ddot{\theta}_i$, $\ddot{w}_{ci}$, and $\ddot{u}_{ci}$ at time $t+\Delta t$ as performed in Step 1.

The circulation from Step 1 to Step 4 is implemented in the time domain by a computer program. The numerical algorithm is provided to calculate the earthquake response of the tall RC chimney, considering eccentricities z_{ci} $(i = 1, 2, \ldots, n)$.

Wilson θ method is used to solve the conventional dynamic equations of equilibrium in which eccentricities are not considered. Their results are called the conventional results in this study.

Here, the rotation of the foundation is not considered.

3. Stability Condition

3.1. Corresponding Relations. For simplicity in deriving the stability condition of the algorithm, we assume that $(\mathrm{EI})_l = (\mathrm{EI})$, $h_l = h$, and $\alpha_l = \alpha$ for all segments. Axial force N_l is omitted in K_{jl} $(j = 1, 2, \ldots, 5)$. Eccentric phenomena are neglected in equation (3); and $m_i = m$ and $J_{ci} = J_i = J$ for all investigated lumps. On the basis of these assumptions, vertical governing equations are decoupled from the governing equations of transverse and rotational deformations. Thus, we only study the coupling equations of transverse and rotational deformations to provide the stability condition for the algorithm presented in this study.

On the basis of the above assumption, the corresponding relations between the coefficients used in Timoshenko beam theory and those used in the proposed algorithm are as follows (see Appendix A):

$$\begin{aligned} \rho_0 A_0 &\Longleftrightarrow \frac{m}{h}, \\ \mathrm{GA}_s &\Longleftrightarrow K \cdot h, \\ \rho_0 I &\Longleftrightarrow \frac{J}{h}, \\ \mathrm{EI} &\Longleftrightarrow (\mathrm{EI}). \end{aligned} \tag{14}$$

3.2. Stability Condition Based on Timoshenko Beam Model. The flexural wave equation of Timoshenko beam is

$$\frac{\partial^2 u}{\partial^2 t} + C_0^2 R^2 \frac{\partial^4 u}{\partial^4 z} - R^2\left(1 + \frac{C_0^2}{C_Q^2}\right)\frac{\partial^4 u}{\partial^2 z \partial^2 t} + \frac{R^2}{C_Q^2}\frac{\partial^4 u}{\partial^4 t} = 0, \tag{15}$$

where $C_0^2 = (E/\rho_0)$, $R^2 = (I/A_0)$, and $C_Q^2 = (\mathrm{GA}_s/\rho_0 A_0)$.

Substituting a flexural wave $u = u_0 e^{i(\omega t - kz)}$ into the finite difference formula of Equation (15), we obtain the following equation (see equation (A.12) in Appendix A):

$$\begin{aligned} &\frac{4C_0^2R^2}{h^4}\sin^4\frac{kh}{2} - R^2\left(1+\frac{C_0^2}{C_Q^2}\right)\cdot\frac{4}{h^2\Delta t^2}\sin^2\frac{\omega\Delta t}{2}\sin^2\frac{kh}{2} \\ &\quad + \frac{R^2}{C_Q^2}\frac{4}{\Delta t^4}\sin^4\frac{\omega\Delta t}{2} - \frac{1}{\Delta t^2}\sin^2\frac{\omega\Delta t}{2} = 0. \end{aligned} \tag{16}$$

Solving equation (16) with $\sin^2(\omega\Delta t/2)$ as unknown yields the following:

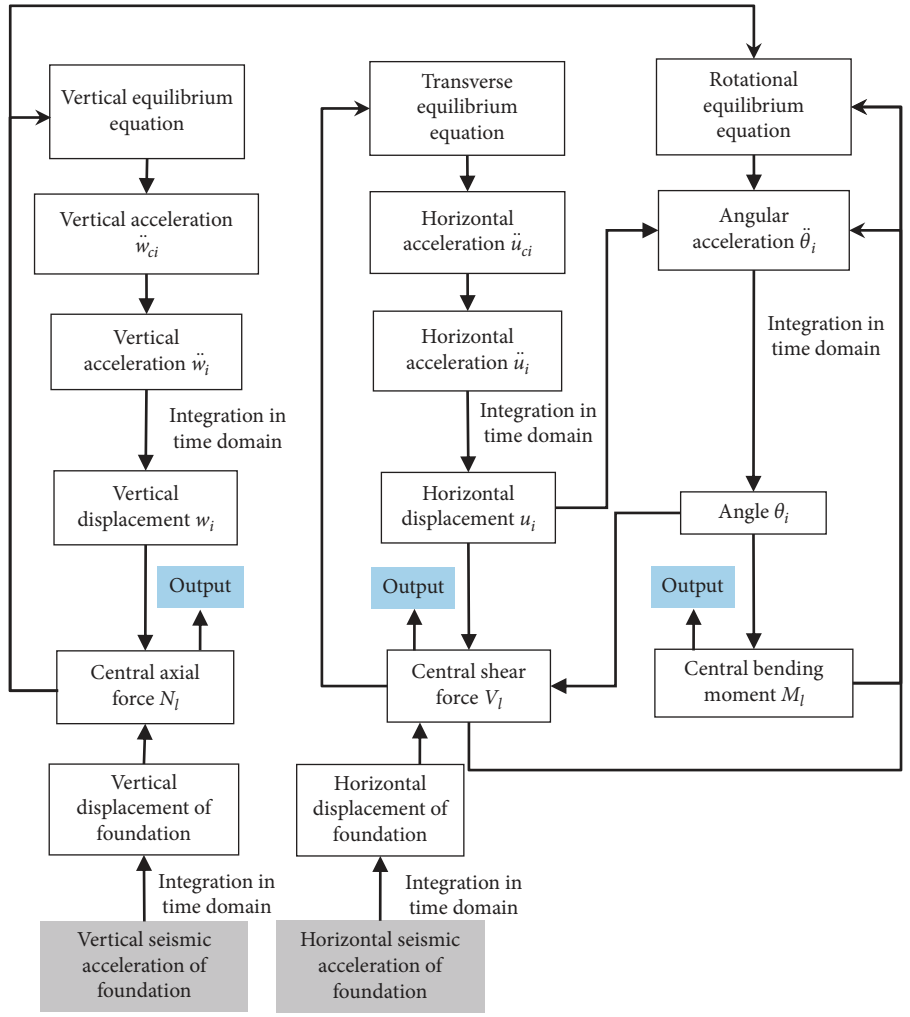

Figure 4: Algorithm description diagram.

$$\sin^2\frac{\omega\Delta t}{2} = \Delta t^2\frac{\left[\left(C_0^2+C_Q^2\right)(4/h^2)\sin^2(kh/2)+\left(C_Q^2/R^2\right)\right] \pm \sqrt{\left[\left(C_0^2+C_Q^2\right)(4/h^2)\sin^2(kh/2)+\left(C_Q^2/R^2\right)\right]^2-\left(\left(8C_0C_Q/h^2\right)\sin^2(kh/2)\right)^2}}{8}. \tag{17}$$

Given $\sin^2(\omega\Delta t/2) \le 1$, we approximately have the following equation (see equation (A.16) in Appendix A):

$$\begin{aligned}\Delta t &\le \frac{h}{\sqrt{\left(C_0^2+C_Q^2\right)\sin^2(kh/2)+\left(C_Q^2h^2/4R^2\right)}} \\ &\le \frac{h}{\sqrt{\left(C_0^2+C_Q^2\right)+\left(C_Q^2h^2/4R^2\right)}}.\end{aligned} \tag{18}$$

3.3. Stability Condition for the Proposed Algorithm. The stability condition used in the algorithm presented in this paper can be provided by using equation (18) and the corresponding relations (14) as follows:

$$\Delta t \le \frac{h}{\sqrt{((\mathrm{EI})h/J)+(12(\mathrm{EI})/mh(1+2\alpha))+(3(\mathrm{EI})h/J(1+2\alpha))}}. \tag{19}$$

4. Method Validation

We study bending wave propagation of a beam to verify the effectiveness of the new algorithm. The beam with equal cross-sectional area is designed to avoid eccentricity. The result given by the finite difference method [29] is used to test the proposed numerical algorithm.

The elastic modulus of the beam is $E = 209$ GPa, density is $\rho = 8000$ kg/m^3, Poisson's ratio is $\nu = 0.3$, and shear cross-sectional correction factor is $k' = 0.886$. The length of the beam is $X = 6.35$ m, and the radius is 0.127 m. The number of discrete segments is 500 in the length direction for the

uniform beam. On the basis of the calculation parameters of the beam, the time step of the beam satisfying the stability condition of the method is $\Delta t \le 1.51\,\mu$s obtained by equation (19), and the calculation time step is $\Delta t = 1.25\,\mu$s.

The length from the left end of the beam is x, and the bending moment at the section is M. After normalization, the time $\overline{t}$ is $(1/X)\sqrt{(E/\rho)}t$, the length is $\overline{x} = (x/X)$, and the bending moment is $\overline{M} = (MX/\mathrm{EI})$.

The inclination moment of the left end of the beam is

$$\overline{M}_1 = \begin{cases} \dfrac{\overline{t}}{\overline{t}_0}, & 0 \le \overline{t} \le \overline{t}_0, \\ 1, & \overline{t} > \overline{t}_0. \end{cases} \tag{20}$$

Figure 5 shows the comparison curves of the bending moments $\overline{M}$ at different cross sections of the beam at $\overline{t} = 7.0554$.

The calculation results of the new numerical method are nearly the same as those of the finite difference method. The comparison results show that the presented algorithm is valid for calculating the earthquake responses of tall RC chimney.

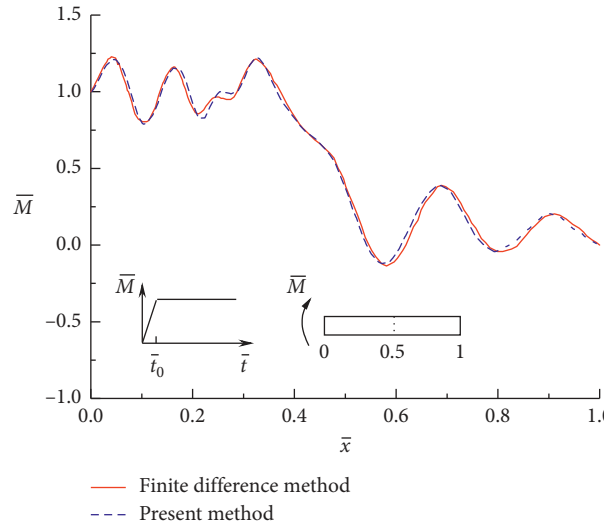

Figure 5: Moment distribution along the length of the uniform beam at $\overline{t} = 7.0554$.

5. Earthquake Responses of Tall RC Chimneys

5.1. Earthquake Records Used. Eleven earthquake acceleration records on four types of soil are used as earthquake load to calculate the structural earthquake response. Four types of soil are denoted by rock, soft rock, stiff soil, and soft soil. Soil type is characterized by shear wave velocity. The corresponding earthquake records are selected from the Pacific Earthquake Engineering Research Center website [30]. Table 1 shows the 11 earthquake records.

According to the peak value of design earthquake acceleration of 8 degrees seismic intensity in the literature [31], the peaks of the horizontal earthquake accelerations are adjusted to 0.2 g in practical calculations. The peaks of the vertical earthquake accelerations are adjusted to 0.13 g. The damping is omitted.

5.2. Two Models of RC Chimneys. Two RC chimneys [32] of 150 m and 210 m height are studied. Figure 6 shows the two models of RC chimneys. (1) The concrete strength grade of the 150 m high RC chimney is C25, and the steel strength grade is HRB335. The outer radius of the bottom is 8.46 m, and the wall thickness is 0.4 m. The outer radius of the top is 3.0 m, and the wall thickness is 0.16 m. The gradient c is 0.1 below 25 m, 0.03 ranging from 25 m to 75 m, and 0.015 ranging from 75 m to 150 m. Table 2 shows the parameters of the 150 m high RC chimney. (2) The concrete strength grade of the 210 m high RC chimney is C35, and the steel strength grade is HRB335. The outer radius of the bottom is 10.6 m, and the wall thickness is 0.6 m. The outer radius of the top is 3.85 m, and the wall thickness is 0.18 m. The gradient c is 0.1 below 30 m, 0.03 ranging from 30 m to 100 m, and 0.015 ranging from 100 m to 210 m. Table 3 shows the parameters of the 210 m high RC chimney. According to the literature [33], the standard value of the compressive strength of C25 concrete is 16.7 N/mm^2, the design value is 11.9 N/mm^2, and the elastic modulus is $E_C = 2.8 \times 10^4$ N/mm^2. The standard value of the compressive strength of C35 concrete is 23.4 N/mm^2, the design value is 16.7 N/mm^2, and the elastic modulus is $E_C = 3.15 \times 10^4$ N/mm^2. The elastic modulus of HRB335 reinforcement is $E_S = 2.0 \times 10^5$ N/mm^2, the standard value of strength (yield strength) is 335 N/mm^2, and the design value of strength is 300 N/mm^2.

The discrete segments are all 10 m long in the vertical direction for each of the two chimneys. Each chimney will become part of such calculated model consisting of several cylinders of different cross-sectional areas because an actual chimney structure has variable cross-sectional areas. Thus, the phenomena of eccentricities between the nodes and the corresponding centroids of the investigated lumps appear in the calculation of the earthquake response of the actual chimney. The mass of each investigated lump consists of half the upper segment and half the lower segment around the discrete node. The moment of inertia of each investigated lump about the horizontal axis through its centroid is calculated. On the basis of the calculation parameters of the 150 m and 210 m high chimneys, the time step satisfying the stability condition of the method is obtained by equation (19), $\Delta t \le 3.4$ ms and $\Delta t \le 3.1$ ms in the 150 m and 210 m high chimneys, respectively. The time step is 1.0 ms.

5.2.1. Effect of Eccentricity. Eleven earthquake waves are used. The effect of eccentricity on normal earthquake stress of the chimney are studied when horizontal and vertical components are inputted simultaneously.

Figure 7 shows the spatial distribution curves of the maximum earthquake normal stresses of different cross sections for the 150 m high chimney under the actions of Landers (No. 1 in Table 1), Loma Prieta (No. 2), Borrego (No. 3), and Chichi (No. 4) waves. Figure 8 shows the comparison curves of the 210 m high chimney. "New"

Table 1: Earthquake records used.

Serial number	Soil types	Earthquake	Date	Direction	Station and component	PGA (g)
No. 1	Rock	Landers	1992/06/28	Horizontal	LANDERS/ABY000	0.115
				Vertical	LANDERS/ABY-UP	0.090
No. 2	Soft rock	Loma Prieta	1989/10/18	Horizontal	LOMAP/CLS000	0.644
				Vertical	LOMAP/CLS-UP	0.455
No. 3	Stiff soil	Borrego	1942/10/21	Horizontal	BORREGO/B-ELC000	0.033
				Vertical	BORREGO/B-ELC-UP	0.068
No. 4	Soft soil	Chichi	1999/09/20	Horizontal	CHICHI/CHY004-N	0.100
				Vertical	CHICHI/CHY004-V	0.041
No. 5	Rock	Morgan Hill	1984/04/24	Horizontal	MORGAN/G01230	0.069
				Vertical	MORGAN/G01-UP	0.092
No. 6	Soft rock	Loma Prieta	1989/10/18	Horizontal	LOMAP/GGB360	0.123
				Vertical	LOMAP/GGB-UP	0.056
No. 7	Stiff soil	Chichi	1999/09/20	Horizontal	CHICHI CHY028-N	0.821
				Vertical	CHICHI CHY028-V	0.337
No. 8	Stiff soil	Chichi	1999/09/20	Horizontal	CHICHI TCU076-N	0.416
				Vertical	CHICHI TCU076-V	0.281
No. 9	Stiff soil	Morgan Hill	1984/04/24	Horizontal	MORGAN/G03090	0.200
				Vertical	MORGAN/G03-UP	0.395
No. 10	Stiff soil	Morgan Hill	1984/04/24	Horizontal	MORGAN HVR240	0.312
				Vertical	MORGAN HVR-UP	0.110
No. 11	Soft soil	Imperial Valley	1079/10/15	Horizontal	IMPVALL H-E03140	0.266
				Vertical	IMPVALL H-E03-UP	0.127

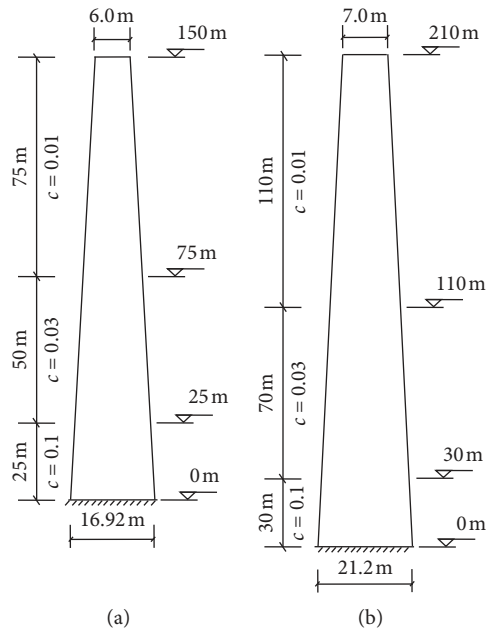

Figure 6: Model of (a) 150 m and (b) 210 m high chimneys.

denotes that the phenomena of eccentricities are considered. "Conventional" denotes the conventional results, in which the phenomena of eccentricities are neglected, for the earthquake responses of the real RC chimneys. Dashed lines ("tensile") denote tensile stresses, whereas solid lines ("press") denote compressive stresses.

A comparison of the red solid lines and the blue solid lines in Figures 7 and 8 shows that the increased phenomena of peak values of the normal compressive stresses appear when eccentricities are considered.

A comparison of the red dashed lines and the blue dashed lines in Figures 7 and 8 shows that the increased phenomena of peak values of the normal tensile stresses appear when eccentricities are considered.

Table 4 shows the details of the increase in percentage of maximum earthquake normal tensile/compressive stresses when phenomena of eccentricities are considered.

Table 5 shows maximum earthquake compressive stress, mean value, and standard deviation of different sections of the 150 m high chimney under 11 earthquake

Table 2: Parameters of 150 m high RC chimney.

Elevation (m)	Outer radius (m)	Wall thickness (m)	Reinforcement ratio (%)
150	3.00	0.16	0.45
137.5	3.52	0.16	0.47
125	3.71	0.16	0.47
112.5	3.89	0.18	0.42
100	4.08	0.18	0.42
87.5	4.27	0.22	0.47
75	4.46	0.22	0.47
62.5	4.83	0.26	0.52
50	5.21	0.26	0.52
37.5	5.58	0.34	0.50
25	5.96	0.34	0.50
5	7.96	0.40	0.52
0	8.46	0.40	0.52

Table 3: Parameters of 210 m high RC chimney.

Elevation (m)	Outer radius (m)	Wall thickness (m)	Reinforcement ratio (%)
210	3.50	0.18	0.57
190	4.15	0.18	0.57
170	4.45	0.20	0.51
150	4.75	0.20	0.67
130	5.05	0.20	0.67
120	5.20	0.23	0.74
110	5.35	0.26	0.65
100	5.50	0.29	0.58
90	5.80	0.32	0.65
80	6.10	0.35	0.60
70	6.40	0.38	0.67
60	6.70	0.41	0.62
50	7.00	0.44	0.74
40	7.30	0.47	0.70
30	7.60	0.50	0.65
16.5	8.95	0.53	0.77
0	10.60	0.60	0.68

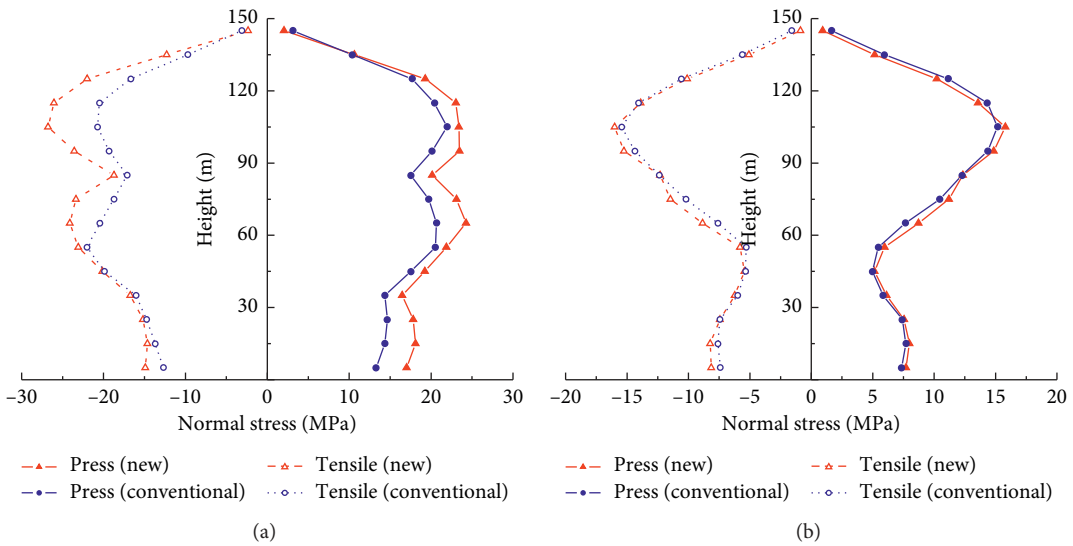

Figure 7: Continued.

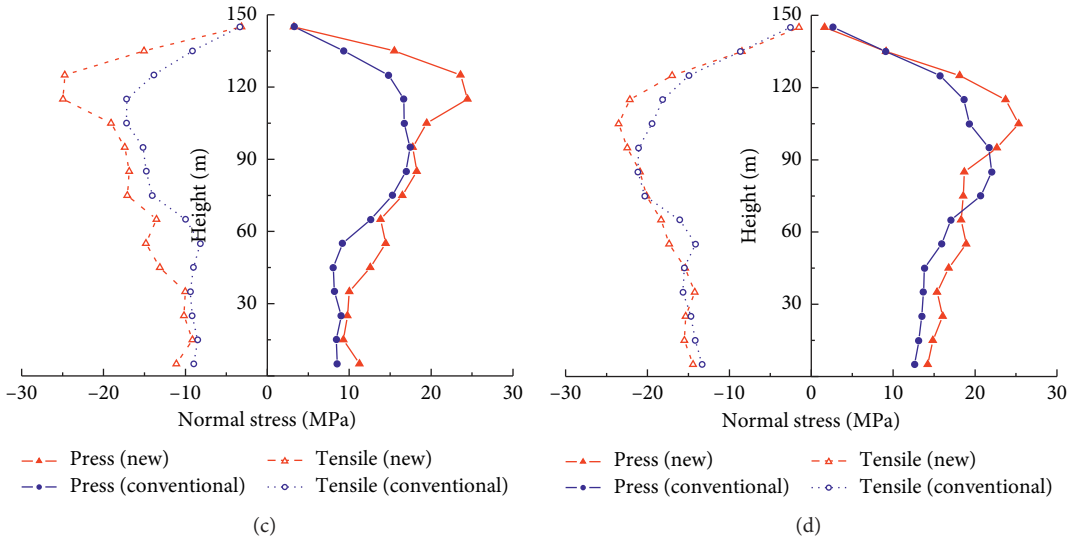

Figure 7: Spatial distributions of maximum earthquake normal stresses at different cross sections of the 150 m high chimney under four earthquake wave actions: (a) Landers wave (No. 1 in Table 1); (b) Loma Prieta wave (No. 2); (c) Borrego wave (No. 3); (d) Chichi wave (No. 4).

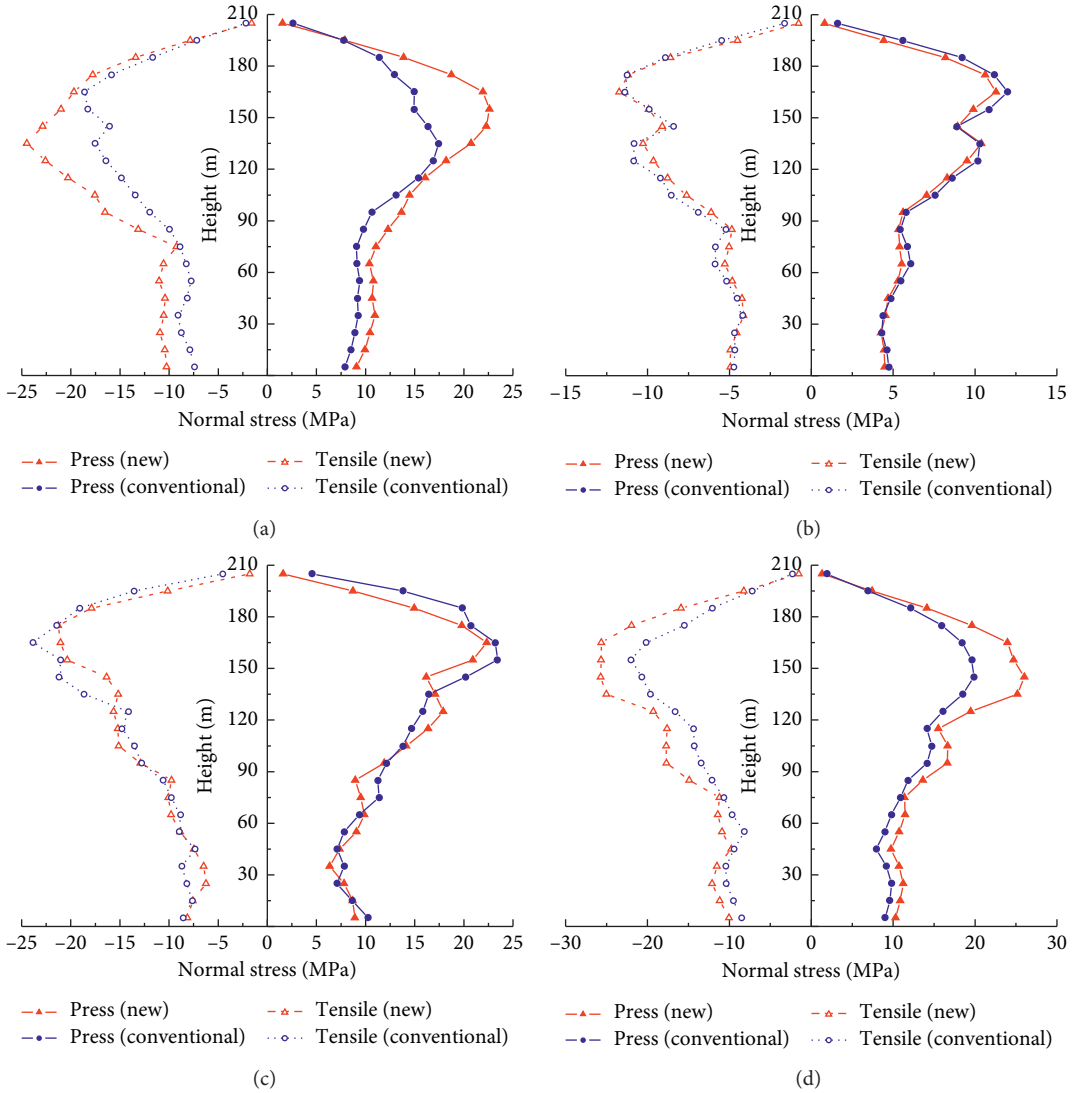

Figure 8: Spatial distributions of maximum earthquake normal stresses at different cross sections of the 210 m high chimney under four earthquake wave actions: (a) Landers wave (No. 1); (b) Loma Prieta wave (No. 2); (c) Borrego wave (No. 3); (d) Chichi wave (No. 4).

Table 4: Percentages of increase in maximum earthquake normal stresses.

Seismic waves	Maximum earthquake normal stresses increased			
	150 m		210 m	
Landers (No. 1)	7% (compressive)	29% (tensile)	30% (compressive)	31% (tensile)
Loma Prieta (No. 2)	4% (compressive)	4% (tensile)	−6% (compressive)	3% (tensile)
Borrego (No. 3)	40% (compressive)	45% (tensile)	−5% (compressive)	−11% (tensile)
Chichi (No. 4)	15% (compressive)	11% (tensile)	31% (compressive)	17% (tensile)

Table 5: Maximum earthquake compressive stresses of the 150 m high chimney under the action of 11 earthquake waves considering vertical eccentricities.

High	Serial number												
	1	2	3	4	5	6	7	8	9	10	11	Mean	Standard deviation
5	17.010	7.717	11.246	14.230	3.482	10.097	5.921	7.997	3.671	6.339	7.160	8.625	4.215
15	18.103	7.988	9.306	14.845	2.561	10.899	6.311	8.594	3.176	6.847	7.752	8.762	4.583
25	17.811	7.554	9.795	16.047	2.853	11.025	6.220	7.992	3.318	6.901	9.003	8.956	4.662
35	16.475	6.128	10.006	15.363	3.864	9.321	5.186	7.083	4.455	6.180	8.760	8.438	4.190
45	19.225	5.138	12.582	16.774	5.095	6.611	4.861	6.217	4.728	4.847	8.994	8.643	5.222
55	21.856	5.972	14.454	18.917	4.458	7.092	5.830	6.942	4.052	4.971	8.281	9.348	6.172
65	24.280	8.720	13.826	18.302	4.572	12.040	7.450	9.123	4.556	6.848	9.922	10.876	6.010
75	23.119	11.202	16.489	18.571	5.310	16.889	8.408	11.441	5.503	10.154	11.935	12.638	5.573
85	20.135	12.336	18.254	18.691	4.395	19.644	8.477	12.966	5.251	11.897	12.518	13.142	5.579
95	23.456	14.853	17.752	22.674	5.197	21.044	9.936	15.339	6.017	13.187	12.684	14.740	6.205
105	23.388	15.798	19.462	25.328	5.928	20.219	10.333	17.028	6.852	13.349	11.428	15.374	6.429
115	23.024	13.572	24.448	23.733	7.695	16.853	9.306	14.868	7.790	12.157	10.025	14.861	6.370
125	19.287	10.223	23.603	18.134	8.715	11.734	7.027	11.008	7.465	9.020	8.885	12.282	5.508
135	10.645	5.170	15.509	9.135	6.332	5.451	3.760	6.105	4.277	4.523	5.318	6.929	3.522
145	2.028	0.928	3.245	1.614	1.427	0.880	0.714	1.370	0.909	0.823	1.085	1.366	0.740

Table 6: Maximum earthquake compressive stresses of the 150 m chimney under the action of 11 earthquake waves ignoring vertical eccentricities.

High	Serial number												
	1	2	3	4	5	6	7	8	9	10	11	Mean	Standard deviation
5	13.289	7.369	8.554	12.633	3.384	10.305	5.134	7.313	3.331	5.934	6.745	7.636	3.341
15	14.345	7.691	8.419	13.151	2.551	11.081	5.622	7.949	2.885	5.974	7.481	7.923	3.773
25	14.663	7.413	9.033	13.475	2.504	11.043	5.951	7.640	3.002	5.274	8.561	8.051	3.902
35	14.349	5.850	8.187	13.705	2.992	9.354	6.185	6.321	3.458	5.063	8.813	7.661	3.731
45	17.519	4.976	8.059	13.816	4.116	7.107	6.016	6.577	3.657	4.618	8.719	7.744	4.307
55	20.530	5.451	9.178	15.920	4.751	7.269	6.060	7.221	3.133	4.536	8.345	8.400	5.264
65	20.660	7.658	12.663	17.034	3.858	11.333	7.614	8.218	3.604	6.526	9.731	9.900	5.263
75	19.725	10.469	15.268	20.713	4.605	15.857	8.474	9.739	5.055	8.741	11.681	11.848	5.426
85	17.501	12.267	16.931	22.010	4.934	18.636	8.167	10.660	5.284	10.439	12.392	12.656	5.552
95	20.104	14.349	17.435	21.680	5.011	20.800	8.797	12.931	5.334	11.404	12.197	13.640	5.891
105	21.951	15.170	16.700	19.318	5.453	20.830	9.370	15.129	5.800	10.514	11.032	13.752	5.745
115	20.385	14.337	16.688	18.629	7.109	18.066	8.969	14.270	6.014	8.398	9.452	12.938	5.122
125	17.655	11.136	14.798	15.712	7.554	13.324	7.386	10.924	5.278	6.956	8.047	10.797	4.106
135	10.348	5.974	9.327	9.096	5.879	6.914	4.598	6.387	3.223	4.267	4.705	6.429	2.300
145	3.091	1.632	3.315	2.693	2.384	1.875	1.460	2.273	1.196	1.333	1.554	2.073	0.728

wave actions when vertical eccentricities are considered. Table 6 shows maximum earthquake compressive stress, mean value, and standard deviation when vertical eccentricities are ignored.

In Table 5, the comparison of the data shows that the maximum earthquake compressive stress obtained under different earthquake waves is significantly different, and the degree of the difference can be expressed by the standard deviation. To quantify the degree of difference, its standard deviation S is

$$S = \sqrt{\frac{\sum_{l=1}^{n} (\sigma_l - \overline{\sigma})^2}{n-1}}, \tag{21}$$

where n is the number of samples, that is, the number of selected earthquake waves; σ_l is normal stress on the central section of segment l, that is, the sum of bending stress and axial stress, which is $\sigma_l = (M_l/W_l) + (N_l/A_l)$; W_l is the bending-resistance modulus of the segment l; and $\overline{\sigma}$ is the mean normal stress of the central section.

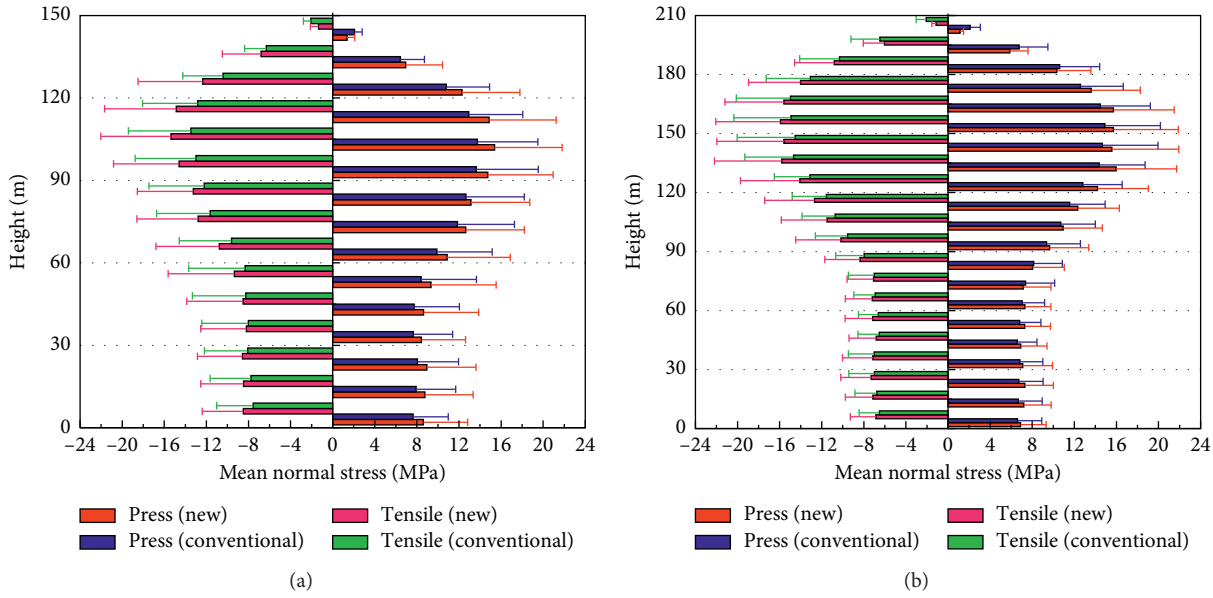

Figure 9: Comparisons of mean and standard deviation of the normal stress of chimney: (a) 150 m high chimney; (b) 210 m high chimney.

Table 7: Maximum earthquake tensile stresses of the 150 m high chimney considering vertical eccentricities.

High	Serial number												
	1	2	3	4	5	6	7	8	9	10	11	Mean	Standard deviation
5	−14.899	−8.142	−11.107	−14.432	−3.545	−10.385	−5.515	−7.845	−3.068	−7.032	−7.351	−8.484	3.918
15	−14.643	−8.224	−9.130	−15.498	−3.170	−11.141	−6.012	−8.139	−2.637	−7.093	−7.417	−8.464	4.079
25	−15.184	−7.429	−10.161	−15.337	−2.699	−11.614	−6.114	−8.303	−2.496	−6.597	−8.329	−8.569	4.290
35	−16.726	−6.233	−10.023	−14.233	−2.904	−9.964	−5.454	−7.328	−2.928	−5.911	−8.414	−8.193	4.345
45	−20.149	−5.441	−13.105	−15.379	−3.684	−7.288	−5.441	−5.944	−3.742	−5.080	−8.275	−8.502	5.371
55	−23.087	−5.802	−14.819	−17.339	−3.907	−7.209	−6.053	−6.328	−4.228	−4.772	−9.252	−9.345	6.296
65	−24.106	−8.842	−13.522	−18.325	−4.194	−11.620	−6.900	−8.679	−4.588	−6.925	−10.773	−10.770	6.021
75	−23.367	−11.458	−17.079	−20.100	−5.300	−16.431	−8.021	−11.427	−5.875	−10.037	−11.643	−12.794	5.798
85	−18.712	−12.305	−16.848	−20.900	−5.449	−19.142	−8.437	−12.990	−5.350	−12.505	−12.969	−13.237	5.330
95	−23.568	−15.257	−17.401	−22.463	−5.488	−20.761	−9.536	−14.479	−5.326	−13.449	−12.741	−14.588	6.229
105	−26.781	−16.007	−19.081	−23.512	−6.008	−19.810	−10.048	−15.935	−6.174	−12.991	−12.563	−15.356	6.669
115	−26.059	−13.898	−24.943	−22.161	−7.670	−16.399	−9.067	−14.409	−6.982	−11.603	−10.365	−14.869	6.797
125	−21.997	−10.105	−24.736	−16.982	−8.222	−11.353	−6.804	−10.998	−7.044	−8.738	−8.935	−12.356	6.136
135	−12.284	−5.071	−15.064	−8.473	−5.732	−5.321	−3.660	−5.796	−4.293	−4.246	−4.992	−6.812	3.667
145	−2.349	−0.883	−3.139	−1.509	−1.387	−0.863	−0.744	−1.380	−0.862	−0.817	−0.948	−1.353	0.757

Table 8: Maximum earthquake tensile stresses of the 150 m high chimney ignoring vertical eccentricities.

High	Serial number												
	1	2	3	4	5	6	7	8	9	10	11	Mean	Standard deviation
5	−12.713	−7.405	−8.992	−13.313	−3.442	−10.154	−5.158	−7.275	−2.661	−5.482	−6.441	−7.549	3.476
15	−13.689	−7.593	−8.485	−14.183	−2.785	−10.792	−5.623	−7.339	−2.313	−5.516	−7.092	−7.765	3.883
25	−14.737	−7.445	−9.195	−14.689	−2.622	−11.050	−5.718	−7.167	−2.953	−5.404	−7.922	−8.082	4.101
35	−16.038	−5.984	−9.391	−15.677	−2.783	−9.446	−5.863	−6.125	−3.703	−4.969	−8.241	−8.020	4.412
45	−19.887	−5.361	−9.031	−15.521	−4.038	−7.266	−5.923	−6.521	−3.986	−4.520	−8.731	−8.253	5.066
55	−22.010	−5.296	−8.157	−14.138	−4.718	−7.033	−6.395	−7.338	−3.525	−4.671	−8.345	−8.330	5.348
65	−20.442	−7.589	−9.998	−16.058	−3.955	−11.176	−7.868	−8.750	−3.820	−6.332	−9.822	−9.619	4.957
75	−18.744	−10.206	−14.035	−20.320	−4.984	−15.659	−8.765	−10.409	−5.016	−8.449	−11.561	−11.650	5.078
85	−17.127	−12.362	−14.803	−21.183	−4.995	−18.267	−8.545	−10.835	−4.926	−9.392	−11.886	−12.211	5.259
95	−19.308	−14.363	−15.150	−21.096	−5.158	−20.466	−8.701	−12.565	−4.347	−9.829	−11.888	−12.988	5.778
105	−20.735	−15.441	−17.201	−19.442	−5.141	−21.169	−9.351	−14.565	−4.676	−9.461	−10.996	−13.471	5.938
115	−20.512	−14.054	−17.158	−18.152	−6.723	−18.408	−9.040	−13.521	−5.411	−8.833	−9.374	−12.835	5.232
125	−16.682	−10.576	−13.862	−14.924	−6.909	−13.614	−7.317	−10.586	−5.691	−7.308	−7.275	−10.431	3.814
135	−9.702	−5.606	−9.130	−8.663	−5.585	−7.096	−4.223	−6.238	−4.007	−4.296	−4.774	−6.302	2.067
145	−3.090	−1.589	−3.339	−2.557	−2.419	−1.928	−1.258	−2.233	−1.350	−1.345	−1.680	−2.072	0.717

Table 9: Maximum earthquake compressive stresses of the 210 m high chimney considering vertical eccentricities.

High	Serial number												
	1	2	3	4	5	6	7	8	9	10	11	Mean	Standard deviation
5	9.073	4.481	8.898	10.293	2.941	9.218	3.664	7.445	6.273	6.974	6.646	6.901	2.416
15	9.938	4.449	8.687	10.863	3.229	9.964	3.797	8.021	6.456	7.002	6.773	7.198	2.591
25	10.466	4.260	7.814	11.223	3.642	10.552	3.865	8.428	6.349	6.810	6.874	7.298	2.707
35	10.942	4.536	6.342	10.703	3.143	10.389	3.755	8.574	5.477	6.347	7.981	7.108	2.806
45	10.664	4.682	7.363	9.732	4.033	9.170	3.919	8.081	4.383	5.379	8.613	6.911	2.501
55	10.790	5.288	9.082	10.740	4.553	7.951	4.411	7.829	4.681	5.806	9.083	7.292	2.452
65	10.391	5.523	9.869	11.456	4.298	7.003	4.417	7.768	5.244	5.932	8.403	7.300	2.480
75	11.058	5.397	9.500	11.388	4.244	5.592	4.090	7.069	5.027	6.239	8.873	7.134	2.653
85	12.283	5.330	8.956	13.619	4.035	7.998	4.624	8.426	5.976	8.010	9.112	8.034	3.010
95	13.669	5.604	11.904	16.621	4.800	11.195	5.281	10.340	7.300	9.797	9.709	9.656	3.704
105	14.484	7.044	14.138	16.663	5.771	13.921	5.765	11.962	9.226	10.333	11.088	10.945	3.708
115	16.080	8.297	16.374	15.511	6.376	17.064	6.771	14.798	11.033	10.732	12.649	12.335	3.950
125	18.201	9.514	17.908	19.468	7.501	20.617	7.767	17.874	12.290	11.079	13.899	14.192	4.836
135	20.731	10.387	17.076	25.177	7.543	23.166	8.884	19.191	15.434	13.947	14.108	15.968	5.754
145	22.279	8.930	16.182	26.017	6.539	23.188	8.091	17.090	15.283	14.884	12.716	15.564	6.365
155	22.605	9.904	20.913	24.714	6.672	21.495	8.269	17.399	13.326	15.063	12.582	15.722	6.154
165	21.942	11.283	22.329	23.957	6.477	19.121	8.648	17.038	12.612	13.700	15.753	15.715	5.766
175	18.729	10.621	19.787	19.615	5.954	15.222	8.110	14.354	10.513	11.494	15.196	13.600	4.668
185	13.872	8.191	14.943	14.117	5.435	10.425	6.618	10.449	8.133	8.744	12.918	10.349	3.233
195	7.892	4.429	8.716	7.440	4.429	5.082	3.846	5.557	4.556	4.826	7.781	5.868	1.735
205	1.547	0.811	1.607	1.321	1.283	0.827	0.769	1.046	0.833	0.868	1.611	1.138	0.343

Table 10: Maximum earthquake compressive stresses of the 210 m high chimney ignoring vertical eccentricities.

High	Serial number												
	1	2	3	4	5	6	7	8	9	10	11	Mean	Standard deviation
5	7.913	4.726	10.278	9.045	3.297	7.885	3.325	8.324	5.691	5.556	6.690	6.612	2.301
15	8.491	4.613	8.632	9.591	3.192	8.644	3.575	8.693	5.534	5.858	6.674	6.681	2.270
25	8.928	4.295	7.073	9.821	3.250	9.291	3.594	8.592	6.273	6.019	6.922	6.733	2.306
35	9.236	4.388	7.835	9.172	3.702	9.105	3.628	7.755	6.311	5.957	8.086	6.834	2.166
45	9.185	4.857	7.109	7.923	4.515	8.191	3.885	6.749	5.297	5.549	9.094	6.578	1.871
55	9.400	5.456	7.823	8.987	4.993	7.663	4.080	6.935	4.754	5.110	9.630	6.803	2.022
65	9.131	6.071	9.355	9.790	4.614	6.873	4.019	7.968	5.305	5.143	9.256	7.048	2.137
75	9.085	5.875	11.357	10.901	5.045	5.885	3.444	9.261	5.258	5.004	9.866	7.362	2.765
85	9.804	5.437	11.261	11.823	5.110	8.655	4.133	10.770	6.123	6.690	9.679	8.135	2.726
95	10.652	5.793	12.132	14.150	5.420	11.524	4.778	12.735	7.346	8.406	10.092	9.366	3.211
105	13.107	7.555	13.799	14.715	6.191	13.593	5.764	13.224	8.968	8.992	11.902	10.710	3.289
115	15.388	8.611	14.686	14.126	6.467	15.260	7.159	12.609	9.625	9.462	13.769	11.560	3.359
125	16.887	10.171	15.816	16.068	7.341	17.337	7.958	13.671	9.509	10.761	15.444	12.815	3.741
135	17.439	10.288	16.448	18.511	7.162	19.932	7.987	17.367	12.785	13.289	16.818	14.366	4.357
145	16.328	8.887	20.181	19.843	6.132	20.116	6.912	19.538	14.792	14.446	13.972	14.650	5.294
155	14.935	10.856	23.421	19.606	6.668	18.987	7.166	19.462	15.096	14.097	13.785	14.916	5.274
165	14.959	11.991	23.222	18.400	7.429	16.611	7.161	18.445	14.258	12.321	14.319	14.465	4.759
175	12.915	11.174	20.729	15.953	6.914	13.073	6.393	14.984	11.878	9.970	14.322	12.573	4.082
185	11.388	9.186	19.862	12.126	7.682	9.282	5.618	11.792	9.435	7.435	12.891	10.609	3.793
195	7.752	5.577	13.811	6.922	6.482	5.034	3.681	7.045	5.408	4.287	8.232	6.748	2.736
205	2.573	1.600	4.560	1.897	2.434	1.349	1.189	2.327	1.491	1.240	2.438	2.100	0.967

The right side of Figure 9(a) is the comparison of the mean values of earthquake compressive stresses between Tables 5 and 6 and the corresponding standard deviation. The left side of Figure 9(a) is the comparisons of the mean values of earthquake tensile stresses and the corresponding standard deviation. The data in Tables 7 and 8 (see Appendix B) are provided regarding maximum earthquake tensile stress, mean value, and standard deviation of the 150 m high chimney when considering vertical eccentricities and neglecting vertical eccentricities. In Figure 9(a), the red and pink columns are, respectively, the mean values of earthquake compressive and tensile stresses considering vertical eccentricities. The blue and green columns are, respectively, the mean values of earthquake compressive and tensile stress neglecting vertical eccentricities. The red and pink lines are, respectively, the standard deviations of different earthquake compressive and tensile stresses considering vertical eccentricities. The blue and green lines are the standard

Table 11: Maximum earthquake tensile stresses of the 210 m high chimney considering vertical eccentricities.

High	Serial number												
	1	2	3	4	5	6	7	8	9	10	11	Mean	Standard deviation
5	−10.262	−4.948	−8.135	−10.034	−2.895	−8.930	−3.943	−7.722	−5.298	−6.667	−6.588	−6.857	2.424
15	−10.435	−4.938	−7.568	−11.181	−2.919	−9.723	−4.201	−8.217	−5.552	−6.907	−6.881	−7.138	2.630
25	−10.935	−4.554	−6.246	−12.106	−3.241	−10.269	−4.221	−8.691	−6.122	−6.946	−7.151	−7.317	2.884
35	−10.553	−4.145	−6.472	−11.522	−3.273	−10.373	−3.642	−8.527	−5.875	−6.486	−7.779	−7.150	2.868
45	−10.408	−4.240	−7.468	−9.756	−4.018	−9.579	−3.551	−7.277	−4.746	−5.330	−8.867	−6.840	2.562
55	−11.024	−4.832	−8.860	−10.900	−4.600	−8.365	−3.709	−6.914	−4.711	−5.920	−9.001	−7.167	2.610
65	−10.567	−5.284	−9.795	−11.400	−4.375	−6.960	−3.870	−7.157	−4.987	−6.342	−8.445	−7.198	2.563
75	−9.261	−5.017	−10.066	−11.198	−4.483	−5.807	−3.879	−7.801	−5.100	−6.042	−9.195	−7.077	2.520
85	−13.145	−4.857	−9.754	−14.902	−4.693	−8.210	−4.959	−7.609	−6.291	−8.202	−9.445	−8.370	3.332
95	−16.522	−6.118	−12.903	−17.681	−4.622	−11.390	−5.345	−9.800	−7.187	−10.105	−10.256	−10.175	4.304
105	−17.546	−7.618	−15.135	−17.703	−5.666	−14.323	−6.034	−12.327	−8.284	−10.474	−11.492	−11.509	4.327
115	−20.278	−8.779	−15.214	−17.611	−6.720	−16.912	−6.769	−15.784	−8.848	−10.066	−12.580	−12.687	4.725
125	−22.597	−9.647	−15.636	−19.295	−6.777	−19.980	−7.368	−18.825	−9.581	−9.736	−15.350	−14.072	5.641
135	−24.483	−10.272	−15.168	−25.018	−7.579	−22.450	−8.291	−19.846	−11.195	−12.573	−16.906	−15.798	6.393
145	−22.866	−9.103	−16.355	−25.713	−5.767	−22.516	−8.095	−17.358	−14.228	−14.451	−15.153	−15.600	6.365
155	−20.992	−9.940	−20.354	−25.657	−5.673	−22.139	−8.594	−16.513	−15.972	−14.672	−14.746	−15.932	6.137
165	−19.689	−11.736	−21.039	−25.636	−7.114	−20.421	−9.126	−15.506	−15.183	−13.670	−12.456	−15.598	5.594
175	−17.762	−11.194	−21.276	−21.932	−6.327	−16.354	−8.317	−13.811	−12.043	−11.622	−13.407	−14.004	4.944
185	−13.414	−8.601	−17.871	−15.897	−6.273	−11.122	−6.563	−10.575	−8.266	−8.356	−12.082	−10.820	3.745
195	−7.845	−4.509	−10.141	−8.223	−4.973	−5.357	−3.606	−5.460	−4.672	−4.489	−7.163	−6.040	2.015
205	−1.591	−0.770	−1.794	−1.524	−1.424	−0.845	−0.694	−0.972	−0.819	−0.753	−1.387	−1.143	0.403

Table 12: Maximum earthquake tensile stresses of the 210 m high chimney ignoring vertical eccentricities.

High	Serial number												
	1	2	3	4	5	6	7	8	9	10	11	Mean	Standard deviation
5	−7.404	−4.719	−8.533	−8.527	−3.335	−8.004	−3.635	−7.965	−6.483	−5.570	−7.629	−6.528	1.923
15	−7.867	−4.672	−7.619	−9.499	−3.416	−8.788	−3.696	−8.663	−6.613	−6.051	−7.548	−6.767	2.080
25	−8.776	−4.683	−8.208	−10.373	−3.163	−9.459	−3.540	−9.161	−6.331	−6.333	−6.843	−6.988	2.443
35	−9.086	−4.199	−8.700	−10.468	−3.866	−9.371	−3.766	−8.596	−5.128	−6.099	−7.874	−7.014	2.463
45	−8.183	−4.540	−7.346	−9.431	−4.291	−8.534	−4.033	−7.092	−4.514	−5.405	−8.582	−6.541	2.022
55	−7.768	−5.168	−8.978	−8.164	−4.662	−7.902	−4.170	−6.826	−4.667	−5.156	−9.280	−6.613	1.895
65	−8.262	−5.869	−8.851	−9.653	−4.784	−7.242	−4.073	−7.791	−5.180	−5.147	−9.472	−6.939	2.008
75	−8.876	−5.860	−9.759	−10.681	−4.735	−6.168	−3.488	−8.404	−5.163	−4.789	−9.311	−7.021	2.444
85	−9.957	−5.203	−10.615	−12.112	−5.577	−8.535	−3.543	−10.392	−6.100	−6.789	−8.921	−7.977	2.703
95	−11.990	−6.905	−12.809	−13.458	−5.783	−11.466	−4.556	−12.103	−7.473	−8.771	−9.768	−9.553	3.052
105	−13.475	−8.542	−13.539	−14.303	−6.060	−13.615	−5.865	−12.736	−8.416	−9.708	−11.819	−10.734	3.137
115	−14.847	−9.219	−14.785	−14.387	−6.629	−15.528	−7.442	−12.490	−8.892	−9.946	−13.041	−11.564	3.232
125	−16.430	−10.839	−14.144	−16.638	−7.599	−17.232	−8.242	−15.041	−11.332	−11.355	−15.373	−13.111	3.404
135	−17.538	−10.834	−18.645	−19.642	−6.946	−20.560	−7.990	−17.535	−13.396	−13.107	−15.292	−14.680	4.638
145	−16.080	−8.417	−21.186	−20.686	−6.343	−20.739	−7.896	−19.356	−13.220	−13.720	−12.230	−14.534	5.500
155	−18.273	−9.907	−21.025	−21.991	−5.937	−19.264	−8.263	−19.261	−14.030	−12.955	−13.363	−14.933	5.417
165	−18.640	−11.394	−23.870	−20.157	−6.959	−17.581	−8.305	−17.337	−13.363	−11.784	−15.212	−14.964	5.159
175	−15.885	−11.241	−21.453	−15.522	−7.398	−14.219	−7.484	−14.848	−11.109	−9.557	−15.198	−13.083	4.197
185	−11.686	−8.918	−19.105	−12.072	−6.373	−10.024	−5.830	−10.987	−8.906	−6.633	−12.945	−10.316	3.779
195	−7.186	−5.468	−13.557	−7.196	−5.199	−5.307	−3.738	−6.277	−5.492	−3.635	−8.202	−6.478	2.734
205	−2.180	−1.625	−4.540	−2.291	−2.251	−1.383	−1.265	−2.016	−1.692	−1.025	−2.601	−2.079	0.950

deviations of different earthquake compressive and tensile stresses neglecting vertical eccentricities. Figure 9(b) shows the case of the 210 m high chimney (data in Tables 9–12).

Figure 9 shows that the earthquake normal stresses increase evidently when considering vertical eccentricities. Significant differences of the maximum earthquake normal stress are observed under different seismic waves actions.

Figure 10 is the boxplot of the maximum earthquake compressive stress distribution at different cross sections of 150 m and 210 m high chimneys under different seismic wave actions when considering eccentricities. They show the mean value, minimum, maximum, and 25%–75% of earthquake compressive stresses. The distribution characteristics of the earthquake compressive stress data are also shown in the figures. The stress distributions near the bottom of the chimney are relatively intensive, whereas those at the middle and upper parts of the chimney are relatively scattered.

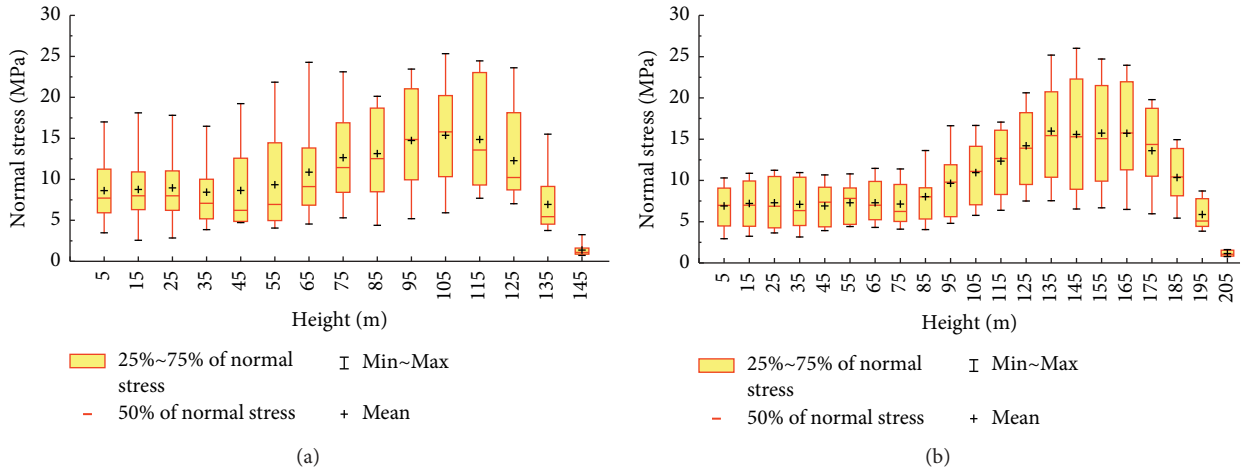

Figure 10: Boxplot of the compressive stress distribution of chimney considering eccentricities: (a) 150 m high chimney; (b) 210 m high chimney.

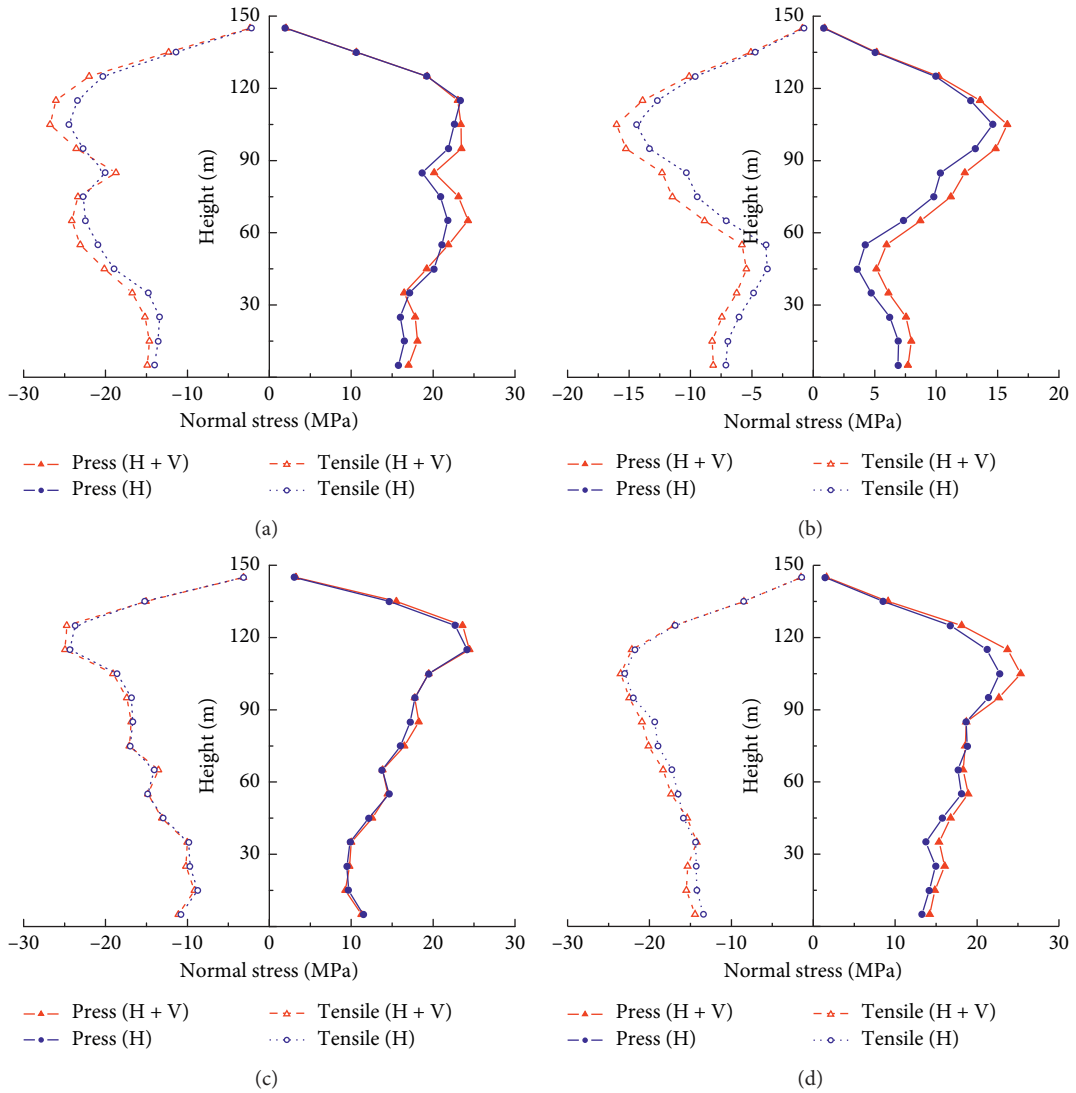

Figure 11: Spatial distributions of maximum earthquake normal stresses at different cross sections for the 150 m high chimney under two types of seismic load applied for each of the four earthquake wave actions: (a) Landers wave (No. 1); (b) Loma Prieta wave (No. 2); (c) Borrego wave (No. 3); (d) Chichi wave (No. 4).

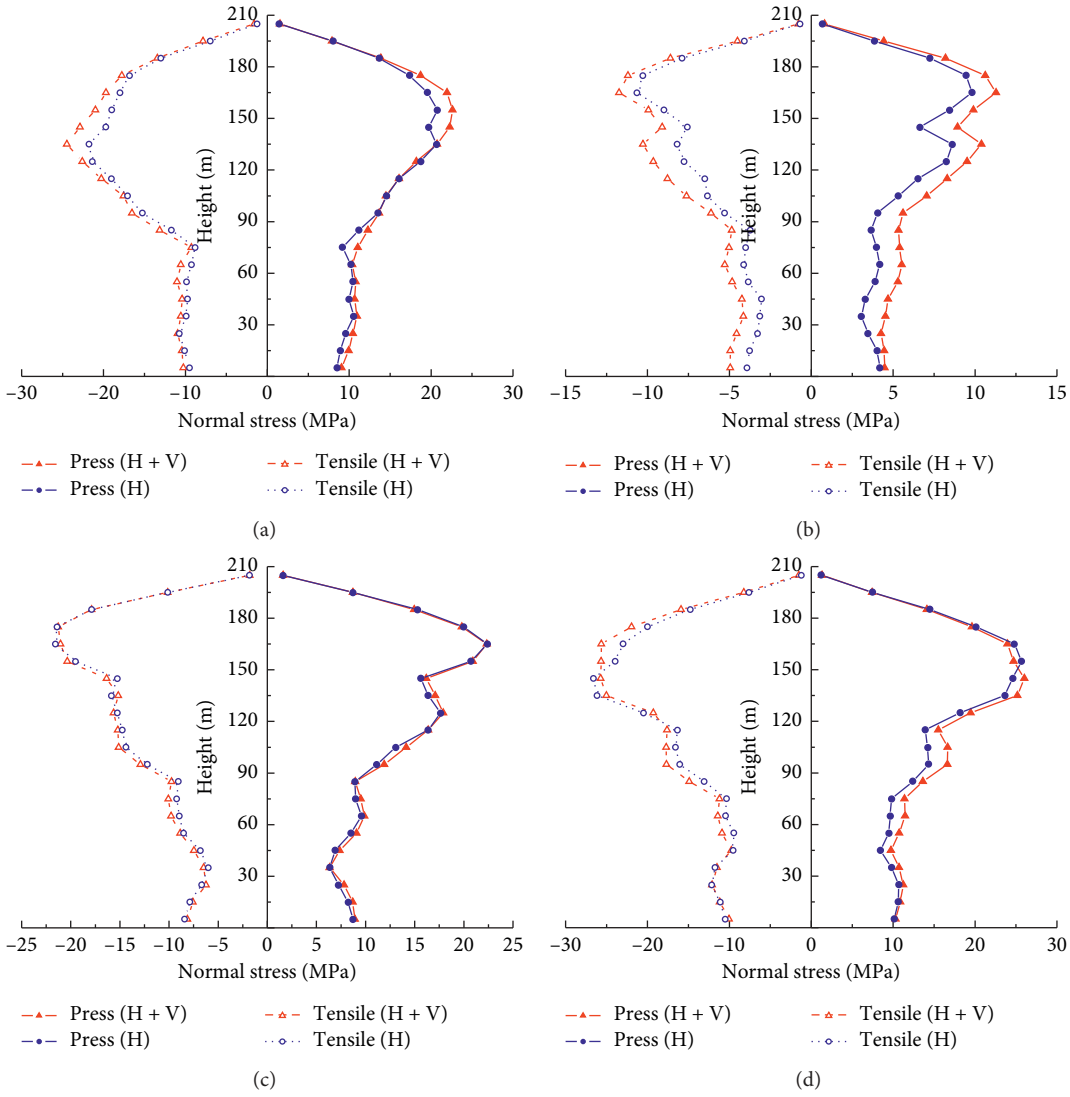

Figure 12: Spatial distributions of maximum earthquake normal stresses at different cross sections for the 210 m high chimney under two types of seismic load applied for each of the four earthquake wave actions: (a) Landers wave (No. 1); (b) Loma Prieta wave (No. 2); (c) Borrego wave (No. 3); (d) Chichi wave (No. 4).

The results studied above show that significant differences of maximum earthquake normal stress under different earthquake wave actions. The comparisons demonstrate that the conventional results (eccentricities neglected) might be less than their actual tensile/compressive stresses in the seismic control cross section of the chimneys under the actions of several specific earthquake waves. The calculation results show that eccentricities between the spatial discrete nodes and the corresponding centroids of investigated lumps should be considered in earthquake response of tall RC chimneys to obtain accurate calculation results.

5.2.2. Effects of Vertical Earthquake. The phenomena of eccentricities are considered to study the effect of vertical earthquake on earthquake normal stresses. Two types of seismic load are applied for each of the four earthquake waves. In the first case, the combined horizontal and vertical earthquake waves (see red lines in Figures 11 and 12) are inputted. In the second case, only the horizontal earthquake wave (see blue lines in Figures 11 and 12) is inputted.

For the 150 m high chimney, Figure 11 shows that the peak normal tensile stress increases by 4% for the Landers wave (No. 1) and 10% for the Loma Prieta wave (No. 2) if vertical earthquake waves are considered. The peak normal compressive stress increases by 7% for the Loma Prieta wave (No. 2) and 10% for the Chichi wave (No. 4) if vertical earthquake waves are considered.

For the 210 m high chimney, Figure 12 shows that the peak normal tensile stress increases by 12% for the Landers wave (No. 1) and 9% for the Loma Prieta wave (No. 2) if vertical earthquake waves are considered. The peak normal compressive stress increases by 9% for Landers wave (No. 1) and 13% for Loma Prieta wave (No. 2) if vertical earthquake waves are considered.

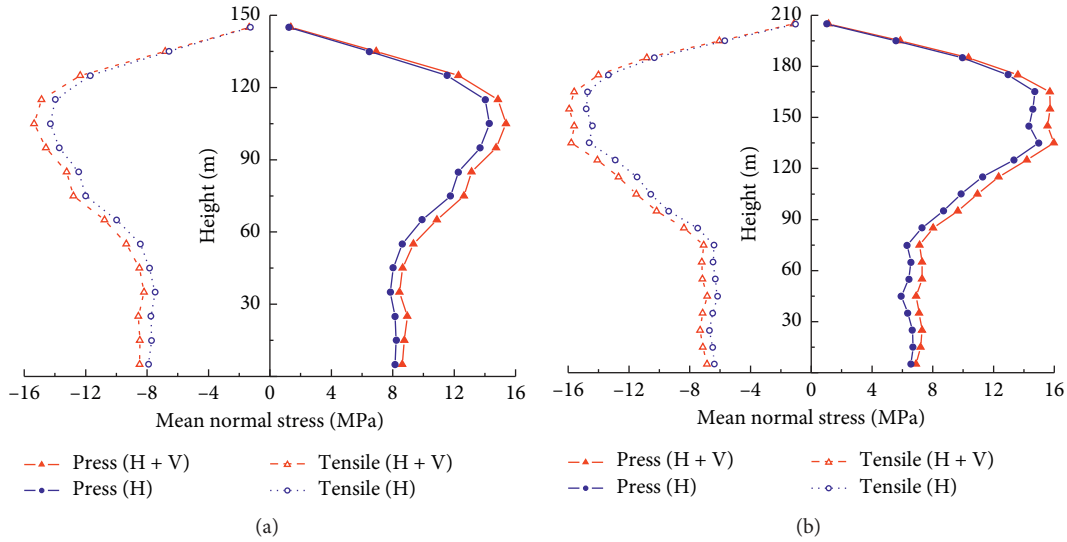

Figure 13: Comparison curve of the mean value of maximum earthquake normal stresses for chimneys under two types of seismic load: (a) 150 m high chimney; (b) 210 m high chimney.

Table 13: Maximum earthquake compressive stresses of the 150 m high chimney when only horizontal seismic acceleration is inputted.

High	Serial number												
	1	2	3	4	5	6	7	8	9	10	11	Mean	Standard deviation
5	15.762	6.884	11.475	13.226	2.984	9.720	5.314	7.104	3.694	6.267	7.235	8.151	3.986
15	16.533	6.912	9.673	14.154	2.374	10.375	5.697	7.298	3.395	6.244	7.812	8.224	4.261
25	15.970	6.204	9.464	14.907	2.194	10.292	5.644	6.853	3.049	6.014	9.059	8.150	4.379
35	17.119	4.713	9.862	13.772	2.836	8.412	4.903	6.279	4.110	5.139	9.057	7.837	4.407
45	20.107	3.593	12.133	15.772	4.133	5.642	4.755	5.276	4.437	3.707	8.936	8.045	5.603
55	21.071	4.229	14.646	18.041	3.645	6.161	5.083	6.183	3.713	3.242	8.740	8.614	6.337
65	21.786	7.321	13.780	17.612	3.645	10.790	6.299	8.381	4.823	5.491	9.217	9.922	5.686
75	20.897	9.792	16.022	18.742	4.307	15.863	7.209	10.533	5.855	8.858	11.386	11.769	5.406
85	18.671	10.349	17.184	18.626	3.973	18.579	7.799	11.399	5.396	11.049	12.025	12.277	5.361
95	21.849	13.139	17.782	21.304	4.313	19.716	8.952	13.522	5.751	12.327	12.051	13.701	5.966
105	22.592	14.578	19.457	22.671	4.985	19.364	9.133	14.541	6.688	12.095	11.287	14.308	6.136
115	23.369	12.785	24.161	21.098	7.016	16.249	8.339	12.902	7.520	11.069	9.754	14.024	6.313
125	19.263	9.922	22.706	16.703	7.430	11.274	6.289	9.926	7.222	8.303	7.947	11.544	5.502
135	10.624	5.025	14.653	8.506	5.419	5.190	3.297	5.773	4.065	4.181	4.662	6.490	3.436
145	1.946	0.838	3.020	1.463	1.236	0.789	0.615	1.260	0.848	0.766	0.892	1.243	0.705

Table 14: Maximum earthquake tensile stresses of the 150 m high chimney when only horizontal seismic acceleration is inputted.

High	Serial number												
	1	2	3	4	5	6	7	8	9	10	11	Mean	Standard deviation
5	−14.019	−7.073	−10.794	−13.376	−3.065	−9.883	−5.107	−7.404	−2.917	−6.109	−7.146	−7.899	3.748
15	−13.568	−6.946	−8.764	−14.184	−2.128	−10.529	−5.319	−7.538	−2.438	−6.015	−7.459	−7.717	3.918
25	−13.396	−6.049	−9.673	−14.268	−2.217	−10.586	−5.134	−7.319	−2.751	−5.799	−7.994	−7.744	3.943
35	−14.760	−4.852	−9.829	−14.309	−2.644	−8.895	−4.731	−6.290	−3.085	−5.040	−7.879	−7.483	4.145
45	−18.971	−3.749	−12.950	−15.797	−3.562	−6.153	−4.989	−5.575	−3.317	−3.663	−7.614	−7.849	5.499
55	−20.940	−3.856	−14.872	−16.458	−3.938	−5.793	−5.151	−5.917	−3.675	−3.466	−8.690	−8.432	6.123
65	−22.465	−7.073	−14.037	−17.207	−3.647	−10.650	−6.376	−8.108	−4.479	−5.484	−10.224	−9.977	5.836
75	−22.721	−9.433	−16.977	−18.920	−4.644	−15.423	−7.684	−10.420	−5.601	−8.588	−11.544	−11.996	5.779
85	−20.043	−10.301	−16.678	−19.349	−4.152	−17.961	−8.200	−11.508	−4.973	−11.015	−12.732	−12.447	5.513
95	−22.737	−13.287	−16.842	−21.924	−5.111	−19.726	−9.137	−12.996	−4.815	−11.834	−12.481	−13.717	6.121
105	−24.485	−14.367	−18.594	−22.963	−5.152	−18.972	−9.762	−13.993	−5.724	−11.670	−11.579	−14.297	6.413
115	−23.410	−12.647	−24.355	−21.682	−6.705	−15.693	−8.900	−12.975	−6.598	−11.093	−9.727	−13.980	6.490
125	−20.313	−9.584	−23.734	−16.823	−7.219	−10.906	−6.540	−9.631	−6.598	−8.641	−8.727	−11.701	5.879
135	−11.408	−4.711	−15.196	−8.484	−5.553	−4.981	−3.266	−5.171	−4.017	−4.446	−5.039	−6.570	3.671
145	−2.166	−0.757	−3.138	−1.419	−1.330	−0.772	−0.624	−1.151	−0.790	−0.775	−0.950	−1.261	0.764

Table 15: Maximum earthquake compressive stresses of the 210 m high chimney when only horizontal seismic acceleration is inputted.

High	Serial number												
	1	2	3	4	5	6	7	8	9	10	11	Mean	Standard deviation
5	8.481	4.199	8.705	10.156	2.007	9.332	3.272	7.522	5.873	6.495	6.213	6.569	2.599
15	8.901	4.019	8.216	10.622	2.225	10.012	3.285	8.055	5.978	6.514	5.906	6.703	2.746
25	9.582	3.469	7.243	10.684	2.446	10.362	3.266	8.297	5.919	6.143	5.912	6.666	2.869
35	10.568	3.052	6.345	9.797	2.526	9.397	2.767	7.913	5.484	5.128	6.954	6.357	2.870
45	9.972	3.302	6.902	8.454	3.223	7.488	2.873	7.388	4.133	4.051	7.458	5.931	2.467
55	10.485	3.886	8.502	9.475	3.529	7.237	3.392	6.915	4.759	4.188	8.276	6.422	2.573
65	10.190	4.154	9.585	9.633	3.223	6.894	3.521	6.782	5.247	4.515	8.447	6.563	2.599
75	9.191	3.988	8.965	9.777	3.536	5.854	3.329	6.980	4.994	4.741	8.090	6.313	2.395
85	11.177	3.643	8.928	12.420	3.799	7.406	3.792	8.005	5.956	6.387	8.570	7.280	2.943
95	13.516	4.035	11.145	14.322	3.448	10.454	4.424	9.272	7.536	7.673	9.883	8.701	3.683
105	14.580	5.302	13.069	14.196	4.576	12.836	5.224	10.651	8.796	8.504	10.711	9.859	3.671
115	16.062	6.498	16.367	13.919	5.366	15.006	6.185	13.698	10.445	8.645	11.724	11.265	4.087
125	18.730	8.256	17.638	18.152	5.275	19.078	7.159	16.475	11.612	10.651	13.545	13.325	5.028
135	20.661	8.608	16.365	23.615	5.444	21.778	8.219	17.456	14.630	14.181	13.650	14.964	5.838
145	19.716	6.626	15.624	24.576	4.835	21.610	7.150	16.670	14.439	14.995	11.521	14.342	6.352
155	20.779	8.409	20.741	25.679	4.079	20.345	6.788	16.586	13.115	14.038	9.833	14.581	6.862
165	19.550	9.803	22.386	24.808	5.578	18.092	7.307	16.231	12.737	12.603	13.035	14.739	6.095
175	17.347	9.451	19.978	20.117	5.357	14.149	7.215	13.845	10.595	11.112	13.379	12.959	4.840
185	13.642	7.253	15.301	14.461	5.160	9.390	5.906	9.742	7.723	8.592	12.240	9.946	3.487
195	7.997	3.857	8.696	7.489	4.402	4.434	3.330	4.899	4.067	4.728	7.289	5.563	1.906
205	1.474	0.668	1.583	1.222	1.160	0.650	0.567	0.936	0.698	0.824	1.336	1.011	0.360

Table 16: Maximum earthquake tensile stresses of the 210 m high chimney when only horizontal seismic acceleration is inputted.

High	Serial number												
	1	2	3	4	5	6	7	8	9	10	11	Mean	Standard deviation
5	−9.499	−3.914	−8.402	−10.528	−2.271	−8.311	−3.147	−6.884	−5.485	−5.603	−6.195	−6.385	2.643
15	−10.088	−3.759	−7.888	−11.120	−2.170	−9.016	−3.276	−7.374	−5.517	−5.617	−5.575	−6.491	2.872
25	−10.735	−3.268	−6.696	−12.154	−2.343	−9.816	−3.359	−8.020	−5.630	−5.495	−6.296	−6.710	3.196
35	−9.917	−3.148	−6.027	−11.745	−2.324	−9.532	−2.986	−7.852	−5.311	−5.431	−7.037	−6.483	3.071
45	−9.763	−3.035	−6.814	−9.538	−3.218	−7.901	−3.112	−7.034	−4.432	−4.657	−8.188	−6.154	2.563
55	−9.887	−3.853	−8.522	−9.456	−3.515	−6.972	−3.159	−6.434	−4.759	−4.555	−8.436	−6.323	2.486
65	−9.276	−4.106	−8.968	−10.471	−3.061	−6.145	−3.460	−7.597	−5.049	−4.824	−8.064	−6.457	2.550
75	−8.813	−4.006	−9.201	−10.360	−3.433	−5.116	−3.316	−8.168	−5.097	−4.562	−8.403	−6.407	2.593
85	−11.696	−3.733	−9.048	−13.089	−3.214	−7.460	−4.127	−7.880	−6.340	−6.498	−9.220	−7.482	3.172
95	−15.283	−5.286	−12.218	−16.060	−3.427	−10.971	−4.632	−9.692	−7.143	−8.267	−10.285	−9.388	4.147
105	−17.060	−6.333	−14.403	−16.566	−4.330	−13.582	−5.322	−11.064	−8.223	−8.519	−10.820	−10.566	4.430
115	−19.059	−6.495	−14.769	−16.340	−5.136	−15.559	−5.968	−14.179	−8.929	−7.669	−12.054	−11.469	4.823
125	−21.359	−7.756	−15.261	−20.501	−5.311	−17.463	−6.259	−17.193	−9.471	−8.103	−13.228	−12.900	5.807
135	−21.802	−8.174	−15.876	−26.142	−5.335	−20.549	−7.745	−18.417	−11.458	−11.799	−13.529	−14.621	6.555
145	−19.722	−7.568	−15.281	−26.594	−4.215	−21.400	−7.706	−16.488	−13.112	−13.520	−12.850	−14.405	6.567
155	−18.995	−9.012	−19.516	−23.940	−4.076	−21.179	−8.472	−16.200	−15.026	−13.612	−12.953	−14.816	5.995
165	−18.022	−10.638	−21.577	−22.969	−5.468	−19.116	−8.724	−16.437	−14.438	−12.906	−11.733	−14.730	5.466
175	−16.832	−10.263	−21.403	−20.010	−5.569	−15.119	−7.902	−14.741	−11.533	−11.518	−11.998	−13.353	4.844
185	−13.024	−7.875	−17.879	−14.764	−5.138	−10.190	−5.783	−11.224	−8.565	−8.835	−10.257	−10.321	3.791
195	−6.944	−4.092	−10.140	−7.591	−4.379	−4.781	−3.151	−5.887	−4.848	−4.741	−5.925	−5.680	1.956
205	−1.261	−0.689	−1.797	−1.221	−1.265	−0.696	−0.591	−1.091	−0.865	−0.805	−1.125	−1.037	0.353

Figure 13 shows the spatial comparison curves of the mean values of the maximum normal earthquake stresses for the 150 m and 210 m high chimneys under two types of seismic load. Figure 13(a) is obtained from the average values of Tables 5, 7, 13, and 14. Figure 13(b) is drawn from the mean values of Tables 9, 11, 15, and 16. Figure 13 shows that the normal stress of the chimney can be increased considering the vertical seismic acceleration.

The results studied above show that the vertical ground motion should not be neglected, especially for tall RC chimneys built on rock sites or soft rock sites.

6. Conclusions

A numerical algorithm that can consider the existing phenomena of eccentricities is presented to calculate the earthquake responses of tall RC chimneys. The numerical results

demonstrate that the tensile and compressive stresses may increase in the seismic control cross sections of the chimneys under the actions of several specific earthquake waves when existing eccentricities are considered. The phenomena of eccentricities should be considered to obtain accurate calculation results of earthquake responses for the seismic designs of tall RC chimneys. The maximum normal stresses of earthquake response appear within the upper half of the chimneys, and their values are considerably larger than those within the lower half of the chimneys. Vertical ground motion should not be neglected, especially for chimneys on rock sites and soft rock sites.

Appendix

A. Corresponding Relations

For simplicity in deriving the stability condition, we assume that $(\mathrm{EI})_l = (\mathrm{EI})$, $h_j = h$, and $\alpha_j = \alpha$ for all segments and $m_i = m$ and $J_i = J$ for all investigated lumps. Axial force N_l is omitted in K_{1l}, K_{2l}, and K_{3l}. Eccentric phenomena are neglected in equation (9). Let z_{ci} be zero. The vertical governing equations are decoupled from the governing equations of transverse and rotational deformations. Thus, we study the equations coupling transverse and rotational deformations to provide the stability condition for the method in this work.

On the basis of the aforementioned assumption, the corresponding equations between the governing equations of Timoshenko theory and the proposed method can be expressed as follows:

$$m\frac{\partial^2 u_i}{\partial t^2} = V_l - V_{l-1} \Longleftrightarrow \rho_0 A_0 \frac{\partial^2 u}{\partial t^2} = \frac{\partial V}{\partial z}, \tag{A.1}$$

$$V_i = K\left(u_{i+1} - u_i - \frac{\theta_i + \theta_{i+1}}{2}h\right) \Longleftrightarrow V = \mathrm{GA}_s\left(\frac{\partial u}{\partial z} - \varphi\right), \tag{A.2}$$

$$J\frac{\partial^2 \varphi_i}{\partial t^2} = (M_l - M_{l-1}) + h\left(\frac{V_l + V_{l-1}}{2}\right) \Longleftrightarrow \rho_0 I\frac{\partial^2 \varphi}{\partial t^2} = \frac{\partial M}{\partial z} + V, \tag{A.3}$$

$$M_i = (\mathrm{EI})\frac{\theta_{i+1} - \theta_i}{h} \Longleftrightarrow M = \mathrm{EI}\frac{\partial \varphi}{\partial z}, \tag{A.4}$$

where $K = (12(\mathrm{EI})/h^3)(1/(1+2\alpha))$.

On the basis of the aforementioned corresponding relations of equations, the corresponding relations between the coefficients used in the continuum Timoshenko beam theory and those used in the proposed method are

$$\begin{gathered}\rho_0 A_0 \Longleftrightarrow \frac{m}{h},\\ \mathrm{GA}_s \Longleftrightarrow Kh,\\ \rho_0 I \Longleftrightarrow \frac{J}{h},\\ \mathrm{EI} \Longleftrightarrow (\mathrm{EI}).\end{gathered} \tag{A.5}$$

Therefore, we have

$$C_0^2 = \frac{E}{\rho_0} = \frac{\mathrm{EI}}{\rho_0 I} \Longleftrightarrow \frac{(\mathrm{EI})}{J/h} = \frac{(\mathrm{EI})h}{J}, \tag{A.6}$$

$$R^2 = \frac{I}{A_0} = \frac{\rho_0 I}{\rho_0 A_0} \Longleftrightarrow \frac{J/h}{m/h} = \frac{J}{m}, \tag{A.7}$$

$$C_Q^2 = \frac{\mathrm{GA}_s}{\rho_0 A_0} \Longleftrightarrow \frac{Kh}{m/h} = \frac{12(\mathrm{EI})}{mh(1+2\alpha)}, \tag{A.8}$$

where I is the moment of inertia of the cross-sectional area with respect to the neutral axis.

A.1. Stability Condition Based on Timoshenko Beam Model The flexural wave equation of Timoshenko beam is

$$\frac{\partial^2 u}{\partial^2 t} + C_0^2 R^2 \frac{\partial^4 u}{\partial^4 z} - R^2\left(1 + \frac{C_0^2}{C_Q^2}\right)\frac{\partial^4 u}{\partial^2 z\,\partial^2 t} + \frac{R^2}{C_Q^2}\frac{\partial^4 u}{\partial^4 t} = 0, \tag{A.9}$$

where $C_0^2 = (E/\rho_0)$, $R^2 = (I/A_0)$, and $C_Q^2 = (\mathrm{GA}_s/\rho_0 A_0)$; E and G are the elastic and shear moduli of the beam, respectively; ρ_0 is the mass density; A_0 is the cross-sectional area; and A_s is the effective cross-sectional area for the shear deformation of the beam.

The finite difference formula of equation (A.9) is

$$\begin{aligned}&\frac{1}{\Delta t^2}\left(u_i^{t+\Delta t} - 2u_i^t + u_i^{t-\Delta t}\right) + \frac{C_0^2 R^2}{h^4}\left[\left(u_{i+2}^t - 2u_{i+1}^t + u_i^t\right) - 2\left(u_{i+1}^t - 2u_i^t + u_{i-1}^t\right) + \left(u_i^t - 2u_{i-1}^t + u_{i-2}^t\right)\right]\\ &- R^2\left(1 + \frac{C_0^2}{C_Q^2}\right)\cdot\frac{1}{h^2\Delta t^2}\left[\left(u_{i+1}^{t+\Delta t} - 2u_i^{t+\Delta t} + u_{i-1}^{t+\Delta t}\right) - 2\left(u_{i+1}^t - 2u_i^t + u_{i-1}^t\right) + \left(u_{i+1}^{t-\Delta t} - 2u_i^{t-\Delta t} + u_{i-1}^{t-\Delta t}\right)\right]\\ &+ \frac{R^2}{C_Q^2}\frac{1}{\Delta t^4}\left[\left(u_i^{t+2\Delta t} - 2u_i^{t+\Delta t} + u_i^t\right) - 2\left(u_i^{t+\Delta t} - 2u_i^t + u_i^{t-\Delta t}\right) + \left(u_i^t - 2u_i^{t-\Delta t} + u_i^{t-2\Delta t}\right)\right] = 0.\end{aligned} \tag{A.10}$$

Assuming a flexural wave $u = u_0 e^{i(\omega t - kz)}$ propagating in the beam and substituting it into equation (A.10), we obtain

$$\begin{aligned}&\frac{1}{\Delta t^2}\left(e^{i\omega\Delta t} + e^{-i\omega\Delta t} - 2\right) + \frac{C_0^2 R^2}{h^4}\left(e^{-2ikh} + e^{2ikh} - 4e^{-ikh} - 4e^{ikh} + 6\right)\\ &- \left(1 + \frac{C_0^2}{C_Q^2}\right)\frac{R^2}{h^2\Delta t^2}\left(e^{i(\omega\Delta t - kh)} + e^{-i(\omega\Delta t - kh)} - 2e^{i\omega\Delta t} - 2e^{-i\omega\Delta t} + e^{i(\omega\Delta t + kh)} + e^{-i(\omega\Delta t + kh)} - 2e^{-ikh} - 2e^{ikh} + 4\right)\\ &+ \frac{R^2}{C_Q^2\Delta t^4}\left(e^{2i\omega\Delta t} + e^{-2i\omega\Delta t} - 4e^{i\omega\Delta t} - 4e^{-i\omega\Delta t} + 6\right) = 0.\end{aligned} \tag{A.11}$$

Given $e^{iz} = \cos z + i\sin z$ and $e^{-iz} = \cos z - i\sin z$, equation (A.11) can be derived as

$$\frac{4C_0^2R^2}{h^4}\sin^4\frac{kh}{2} - R^2\left(1 + \frac{C_0^2}{C_Q^2}\right)\cdot\frac{4}{h^2\Delta t^2}\sin^2\frac{\omega\Delta t}{2}\sin^2\frac{kh}{2} + \frac{R^2}{C_Q^2}\frac{4}{\Delta t^4}\sin^4\frac{\omega\Delta t}{2} - \frac{1}{\Delta t^2}\sin^2\frac{\omega\Delta t}{2} = 0. \tag{A.12}$$

Equation (A.12) is a quadratic equation with unknown $\sin^2(\omega\Delta t/2)$, and its solution can be obtained as follows:

$$\sin^2\frac{\omega\Delta t}{2} = \Delta t^2\frac{\left(\left(C_0^2 + C_Q^2\right)(4/h^2)\sin^2(kh/2) + \left(C_Q^2/R^2\right)\right) \pm \sqrt{\left(\left(C_0^2 + C_Q^2\right)(4/h^2)\sin^2(kh/2) + \left(C_Q^2/R^2\right)\right)^2 - \left(\left(8C_0C_Q/h^2\right)\sin^2(kh/2)\right)^2}}{8}. \tag{A.13}$$

Given $\sin^2(\omega\Delta t/2) \le 1$, the stability condition should be

$$\Delta t^2\frac{\left(\left(C_0^2 + C_Q^2\right)\cdot(4/h^2)\sin^2(kh/2) + \left(C_Q^2/R^2\right)\right) \pm \sqrt{\left[\left(C_0^2 + C_Q^2\right)\cdot(4/h^2)\sin^2(kh/2) + \left(C_Q^2/R^2\right)\right]^2 - \left[\left(8C_0C_Q/h^2\right)\sin^2(kh/2)\right]^2}}{8} \le 1, \tag{A.14}$$

which can be expressed approximately as

$$\Delta t^2\frac{\left(C_0^2 + C_Q^2\right)\cdot(4/h^2)\sin^2(kh/2) + \left(C_Q^2/R^2\right)}{4} \le 1. \tag{A.15}$$

That is,

$$\begin{aligned}\Delta t &\le \frac{h}{\sqrt{\left(C_0^2 + C_Q^2\right)\sin^2(kh/2) + \left(C_Q^2h^2/4R^2\right)}}\\ &\le \frac{h}{\sqrt{\left(C_0^2 + C_Q^2\right) + \left(C_Q^2h^2/4R^2\right)}}.\end{aligned} \tag{A.16}$$

A.2. Stability Condition for the Proposed Algorithm. The stability condition used in the proposed method can be provided by using equation (A.16) and the corresponding relations (i.e., equations (A.6)–(A.8)) as follows:

$$\Delta t \le \frac{h}{\sqrt{((\mathrm{EI})h/J) + (12(\mathrm{EI})/mh(1 + 2\alpha)) + (3(\mathrm{EI})h/J(1 + 2\alpha))}}. \tag{A.17}$$

B. Partial Calculation Results

Table 7 shows the maximum earthquake tensile stresses, mean values, and standard deviations of different sections of the 150 m high chimney under 11 seismic waves when horizontal and vertical seismic accelerations are simultaneously inputted and vertical eccentricities are considered. The results when vertical eccentricities are ignored are shown in Table 8.

Table 9 shows the maximum earthquake compressive stresses, mean values, and standard deviations of different sections of the 210 m high chimney under 11 seismic waves when horizontal and vertical seismic accelerations are simultaneously inputted and vertical eccentricities are considered. The results when vertical eccentricities are ignored are shown in Table 10.

Table 11 shows the maximum earthquake tensile stresses, mean values, and standard deviations of different sections of the 210 m high chimney under 11 seismic waves when horizontal and vertical seismic accelerations are simultaneously inputted and vertical eccentricities are considered. The results when vertical eccentricities are ignored are shown in Table 12.

In view vertical eccentricities, Table 13 shows the maximum earthquake compressive stresses, mean values, and standard deviations of different sections of the 150 m high chimney under 11 seismic waves when only horizontal seismic acceleration is inputted. Table 14 shows the results of maximum earthquake tensile stresses of the 150 m high chimney.

In view of vertical eccentricities, Table 15 shows the maximum earthquake compressive stresses, mean values, and standard deviations of different sections of 210 m chimney under 11 seismic waves when only horizontal seismic acceleration is inputted. Table 16 shows the results of the maximum earthquake tensile stresses of the 210 m high chimney.

Data Availability

The analysis result data used to support the findings of this study are included within the article. The calculation data used to support the findings of this study are available from the corresponding author upon request.

Conflicts of Interest

The authors declare that there are no conflicts of interest.

Acknowledgments

This study was supported in part by the National Natural Science Foundation of China (11672190 and 61673281), Liaoning Province Doctor Startup Fund (201601112), Liaoning Provincial Key Research and Development Program (2018103007), and Qinghai Provincial Key Research and Development Program (2017-NK-107).

Supplementary Materials

"Parameter data of 150 m reinforced concrete chimney.xlsx" is the RC chimney parameter data of 150 m height. "Parameter data of 210 m reinforced concrete chimney.xlsx" is the RC chimney parameter data of 210 m height. "Eleven kinds of earthquake records" are input data, which are used to study the seismic response of chimney structures. (*Supplementary Materials*)

References

[1] Z. P. Liao and F. Wang, "Vertical seismic motion input to structures," *Earthquake Engineering and Engineering Vibration*, vol. 3, no. 2, pp. 74–88, 1983, in Chinese.

[2] J. Liu and L. M. He, "Analysis of seismic response of chimneys to combined horizontal and vertical ground motion," *Earthquake Engineering and Engineering Vibration*, vol. 3, no. 2, pp. 89–98, 1983, in Chinese.

[3] F. Wang and Z. P. Liao, "Wave motion response of chimneys to vertical ground motions," *China Civil Engineering Journal*, vol. 17, no. 1, pp. 12–26, 1984, in Chinese.

[4] Q. Liu, R. Z. Zhou, and W. J. Yuan, "Computation of earthquake transient response of skyscraper structures and study of the dynamic properties," *China Civil Engineering Journal*, vol. 43, no. 5, pp. 63–69, 2010, in Chinese.

[5] S. Ding, Y. J. Wang, and S. J. Zhou, "Fracture test of chimney models subjected to vertical shock," *Earthquake Engineering and Engineering Vibration*, vol. 19, no. 3, pp. 34–36, 1999, in Chinese.

[6] J. Y. Chen, J. Zhou, and H. C. Ma, "Study on model test of highrise chimney subjected to vertical seismic action," *Journal of Building Structures*, vol. 26, no. 2, pp. 87–93, 2005, in Chinese.

[7] W. Huang, P. L. Gould, R. Martinez, and G. S. Johnson, "Nonlinear analysis of a collapsed reinforced concrete chimney," *Earthquake Engineering & Structural Dynamics*, vol. 33, no. 4, pp. 485–498, 2004.

[8] P. L. Gould and W. Huang, "Higher mode effects in the nonlinear static analysis of a collapsed chimney," in *Proceedings of the 2006 Structures Congress*, vol. 2006, p. 19, St. Louis, MO, USA, May 2006.

[9] N. O. Akinci, "An investigation on seismic resistance of reinforced concrete industrial chimneys," in *Proceedings of the 2009 Structures Congress*, pp. 964–971, Austin, TX, USA, April 2009.

[10] W. Huang and P. L. Gould, "3-D pushover analysis of a collapsed reinforced concrete chimney," *Finite Elements in Analysis and Design*, vol. 43, no. 11-12, pp. 879–887, 2007.

[11] V. Lopes, J. M. Guedes, E. Paupério, A. Arêde, and A. Costa, "Ambient vibration testing and seismic analysis of a masonry chimney," *Journal of Building Appraisal*, vol. 5, no. 2, pp. 101–121, 2009.

[12] F. Minghini, G. Milani, and A. Tralli, "Seismic risk assessment of a 50 m high masonry chimney using advanced analysis techniques," *Engineering Structures*, vol. 69, pp. 255–270, 2014.

[13] C. Zhou, X. Zeng, Q. Pan, and B. Liu, "Seismic fragility assessment of a tall reinforced concrete chimney," *The Structural Design of Tall and Special Buildings*, vol. 24, no. 6, pp. 440–460, 2015.

[14] C. D. Zhou, X. L. Zeng, F. Zhao, and H. Zhou, "Seismic fragility analysis for high-rise reinforced concrete chimney," *Earthquake Engineering and Engineering Dynamics*, vol. 36, no. 2, pp. 173–181, 2016, in Chinese.

[15] C. D. Zhou, M. W. Tian, X. Zhang, P. G. Wang, and andX. Ma, "Seismic fragility analysis for high-rise RC chimney considering multi-dimensional seismic actions," *China Civil Engineering Journal*, vol. 50, no. 3, pp. 54–61, 2017, in Chinese.

[16] X. Chen, A. Q. Li, W. R. Cheng, and Y. Wang, "The Adomian decomposition method for dynamic characteristics of high-rise buildings," *Journal of Vibration Engineering*, vol. 26, no. 4, pp. 493–499, 2013, in Chinese.

[17] R. Sancibrian, I. Lombillo, E. G. Sarabia, Y. Boffill, H. Wong, and L. Villegas, "Dynamic identification and condition assessment of an old masonry chimney by using modal testing," *Procedia Engineering*, vol. 199, pp. 3410–3415, 2017.

[18] T. Tatara and B. Ratajewicz, "The selection of a dynamic model of a RC chimney based on in Situ research," in *Proceedings of the International Conference on Experimental Vibration Analysis for Civil Engineering Structures*, pp. 619–630, San Diego, CA, USA, July 2017.

[19] D. Mehta and N. J. Gandhi, "Time response study of tall chimneys under the effect of soil structure interaction and long period earthquake impulse," in *Proceedings of the 14th World Conference on Earthquake Engineering*, Beijing, China, October 2008.

[20] R. Livaoglu, "The numerical and empirical evaluation of chimneys considering soil structure interaction and high-temperature effects," *Soil Dynamics and Earthquake Engineering*, vol. 66, pp. 178–190, 2014.

[21] A. M. Halabian and S. Kabiri, "Effect of foundation flexibility on ductility reduction factors for R/C stack-like structures," *Earthquake Engineering and Engineering Vibration*, vol. 10, no. 2, pp. 277–290, 2011.

[22] S. V. Jisha, B. R. Jayalekshmi, and R. Shivashankar, "3D soil-structure interaction analyses of annular raft foundation of tall RC chimneys under wind load," *Indian Geotechnical Journal*, vol. 44, no. 4, pp. 409–426, 2014.

[23] B. R. Jayalekshmi, S. V. Jisha, and R. Shivashankar, "Analysis of foundation of tall R/C chimney incorporating flexibility of soil," *Journal of the Institution of Engineers (India): Series A*, vol. 98, no. 3, pp. 211–217, 2017.

[24] C. D. Zhou, X. L. Zeng, J. Chen, and B. Liu, "Seismic collapse resistance analysis of tall reinforced concrete chimney," *Engineering Mechanics*, vol. 33, no. 5, pp. 57–65, 2016, in Chinese.

[25] C. D. Zhou, X. L. Zeng, and Q. L. Pan, "Seismic response analysis of high-rise RC chimney including soil-structure interaction," *Earthquake Engineering and Engineering Dynamics*, vol. 36, no. 3, pp. 140–150, 2016, in Chinese.

[26] R. Sarkar, D. Shrimal, and S. Goyal, "Seismic analysis of a 275 m tall RCC multi-flue chimney: a comparison of IS code provisions and numerical approaches," *Advances in Structural Engineering*, vol. 2, pp. 1015–1025, 2015.

[27] J. L. Wilson, "Earthquake response of tall reinforced concrete chimneys," *Engineering Structures*, vol. 25, no. 1, pp. 11–24, 2003.

[28] H. Q. Liu, W. B. Li, R. Y. Wu, and L. F. Yan, "Elastic-plastic seismic response analysis on the special-shaped chimney," *Applied Mechanics and Materials*, vol. 711, pp. 520–524, 2014.

[29] N. S. Abhyankar, "Flexural waves in beams with geometrical and material longitudinal discontinuities," *International Journal of Impact Engineering*, vol. 9, no. 2, pp. 205–222, 1990.

[30] Information on https://ngawest2.berkeley.edu/, Peer Ground Motion Database, Pacific Earthquake Engineering Research Center.

[31] GB50010-2010, *Code for Seismic Design of Buildings*, China Architecture & Building Press, Beijing, China, 2010.

[32] China Architecture & Building Press, *Design Manual of Chimneys*, China Architecture & Building Press, Beijing, China, 1989.

[33] GB50010-2010, *Code for Design of Concrete Structures*, China Architecture & Building Press, Beijing, China, 2015.